ASTRONOMY & ASTROPHYSICS
SUPPLEMENT SERIES

Astron. Astrophys. Suppl. Ser. **133**, 361–380 (1998)

Detection of new emission structures around planetary nebulae⋆

C.T. Hua[1], **M.A. Dopita**[2], **and J. Martinis**[1]

[1] Laboratoire d'Astronomie Spatiale du CNRS, Allée Peiresc, Traverse du Siphon, 13012 Marseille, France
[2] Mt Stromlo & Siding Spring Observatories, Canberra, ACT, Australia

Received April 30; accepted June 26, 1998

Abstract. Deep monochromatic observations are presented for 22 galactic planetary nebulae (PNe) performed through narrow-band interference filters, in the direct imaging mode with i) the New Zealand (MJUO) f/7.8 McLellan telescope, ii) the Observatoire de Haute Provence (OHP) f/6 120-cm telescope, and iii) and the Siding Spring Observatory (SSO) ATT 2.3 metre telescope. Some of them are observed for the first time. Conspicuous secondary structures are detected far around the conventional nebular pictures. Such features could be relics of early mass ejections during the post-AGB phase of the progenitors. Alternatively, they are more plausibly projections of external loops/bubbles of the "bar-bell" shape upon the waist (for face-on PNe). We suggest that such structures (cf. Sh 1-89, Hua 1997) are intrinsic to all PNe. Their apparently diverse morphologies would "simply" result from projections of a same PN intrinsic structure at different view angles onto the plane of sky and with respect to the major axis as well. In addition we report the detection of a new nebula in the field of NGC 3699 (50″ distant). Absolute fluxes are provided for three emission lines.

Key words: planetary nebulae — ISM: structure

1. Introduction

The evolution of asymptotic giant branch (AGB) stars towards the planetary nebula (PN) phase of evolution is characterized by a series of helium shell flashes accompanied by enhanced mass-loss (Vassiliadis & Wood 1994). Thus the AGB stars have initial main-sequence masses of 1 $M_\odot$ to 8 $M_\odot$, but they end up as white dwarfs with a mass of only ~ 0.6 to 1.4 $M_\odot$. In the Vassiliadis and Wood models, much of the mass loss occurs in one or more superwind phases which take place towards the end of the quiescent phases of helium shell flash cycles. Therefore, we might expect that the mass lost and subsequently ionized during the PN phase would appear as a series of shells around the main inner body of the PN.

Such outer structures should be structurally modified in a rather profound way during the PN evolution itself. As a matter of fact, it is commonly accepted that planetary nebula shaping results from the interaction between the stellar envelope ejected during the AGB phase (slow wind), and the fast stellar wind driven out from the central star by radiation pressure during the PN phase itself. In this two-wind model (Kwok et al. 1978), Rayleigh-Taylor instabilities play a role in shaping the outskirts and even the inner regions as well (e.g. Dgani & Soker 1997; Dwarkadas & Balick 1998). Furthermore, bipolar outflows may be set up either as a result of the binary nature of the central star, or as a result of the rotation of the precursor star, assumed to be single. Now, the observations (Hua 1997 and references therein) obviously display a large variety of nebular shapes: from symmetrical homogeneous to irregular and knotty configurations, which could reflect either different stages of evolution (Kwok 1982) or the results of interaction of several mechanisms (Bond & Livio 1990; Pascoli 1992; Chevalier 1994).

Observationally, the presence of secondary structures around some well-known PNe was already suspected long ago (Duncan 1937; Millikan 1974; Kaler 1974). Nonetheless, with photographic plates, their detection remained a difficult task due to their extreme faintness. The advent of high-sensitivity CCD detector technology has made the search for such structures much easier. Observations based on the first generation of CCD detectors (Jewitt et al. 1986; Chu et al. 1987) reported such detections and related the existence of multiple-shell to the evolution of planetary nebulae and their parent central stars. However, in general, these observations were obtained using filters of rather wide bandpasses, so that,

Send offprint requests to: C.T. Hua

⋆ The observations were carried out at the Siding Spring Observatory operated by the Australian National University, Australia. NGC 6853 was observed at the Haute Provence Observatory-CNRS 1.20-m telescope, France.

for instance, the two [NII] emission lines contaminate the proper Hα emission.

In this paper, we present a new set of deep CCD observations performed using very narrow-band interference filters to provide optimum sensitivity for the detection of such outer structures, if and where they exist. We have observed 22 galactic PNe, among them some type I PNe (Peimbert & Peimbert 1983) which, on the basis of their high helium and nitrogen contents, are thought to be derived from massive precursor stars. In their simulation of ellipsoidal PNe taking into account the pole-to-equator density gradient, Zhang & Kwok (1998) found that bipolar and even "butterfly" PNe are likely to have massive progenitors. In the case of the Magellanic Cloud PNe, this has been observationally established to be true (Dopita et al. 1997). In addition to the detection of peripheral (and sometimes outstanding) structures lying far beyond the previously known boundaries of the PN, we also give absolute fluxes in emission lines (namely Hα, [NII]6583 Å and [OIII]5007 Å).

2. The observations

The observations were carried out with CCD imagers on three separate telescopes.The majority of the observations were made with the focal reducing imager at the Nasmyth B f/18 focus of the ATT 2.3 metre telescope operated by the Australian National University at the Australian Siding Spring Observatory (ANU - SSO) during two campaigns (July 1995 - July 1997). This instrument provides an f/3.5 focal ratio at the detector. NGC 6853 (the Dumbbell nebula) was observed with the OHP 120-cm telescope at St Michel l'Observatoire. The image scale and field coverage of the images are very similar for the three instruments: the Nasmyth imager SSO-Tektronix 1024 × 1024 CCD has an image scale of $0.60''/24$ μm-pixel, the f/7.8 1-m McLellan telescope at MJUO with its 380 × 576 CCD offers an image-scale of $0.62''/23$ μm-pixel giving a much smaller field of view ($4'\times 6'$), and the f/6 120-cm telescope in Haute Provence with its Tektronix 1024 × 1024 CCD is characterized by a plate scale of $0.686''/24$ μm-pixel and a larger field of view of $\sim 12'$.

Typically, three exposures of 600s (SSO's data) were made in each filter, which allowed the identification and removal of cosmic ray events. At MJUO and OHP observations were done with 1 hour exposures. Images were bias-subtracted and flat-fielded in the usual way. The flat fields were generally obtained in twighlight to ensure that the illumination across the detector was the same as the sky illumination in the observations. The separate images were offset relative to each other by ~ 1 arcsec, and combined using the IRAF task *imcombine* which allowed to remove detector artifacts such as dead or noisy pixels.

2.1. The interference filters

Most of the published "narrow band" PNe images have been actually obtained with filters having bandpasses of order $\Delta\lambda \approx 50$ Å. Mostly these consist of [OIII]λ5007 Å and Hα images. As a result of the broad bandpass, the nitrogen lines, particularly the [NII]λ6583 Å emission, contaminate the Hα flux, especially for Type I PNe, in which the [NII]λ6583 Å line may in some cases be 4-6 times stronger than the Hα line. Problems may also arise in the case of evolved hydrogen deficient objects such as A 79 (see Jewitt et al. 1987; Schwarz et al. 1992). The interference filters used in the present study have bandwidths $\leq$ 10 Å, and are centred at specific wavelengths suitably selected for investigating nebular ionization structure and/or the PN abundance distribution. These filters are generally mounted directly in front of the detector. Provided that the f-ratios are not too small, f/6 being about the limit with such filters, the bandpass broadening due to the off-axis rays in the beam is negligible. In the case of the Nasmyth B imager, the filters were placed at a 50 mm pupil image in the focal reducer, so that every portion of the field passes through the same region of the filter. This removes the effects of inhomogeneities in the multi-layers, but induces a field-dependent shift in the bandpass. However, this should also be negligible for the filters we used in this study. The image quality was typically $1''.5 - 2''.0$ during the observations.

2.2. The photometric calibration

The CCD responses were calibrated by observing the standard star τ Sco (HD 149438, Tüg 1975), and the "compact" planetary nebula flux standards previously calibrated by Dopita & Hua (1997) using the Nasmyth A spectrograph of the ATT 2.3 metre telescope. The cleaned standard star frames then were used for the ADU counts/absolute flux conversion after airmass correction, sky subtraction and allowance for the filter bandwidths. Absolute fluxes are given in erg cm^{-2} s^{-1} units. Nebular and standard star frames were processed and calibrated using both the IRAF and MIDAS software packages.

2.3. The selected planetary nebulae

The PNe we have chosen to observe were selected from the Acker et al. (1993) Catalogue (hereafter referred to as Acker93). Table 1 lists these objects whose main characteristics were extracted from the Cahn et al. (1992) (CKS92) report where available. Otherwise we have used data from Acker93. We generally have concentrated on the PNe with the largest angular extent, and which are classified as high excitation ([OIII]/F(Hβ) > 7) and are characterized by strong [NII] lines (intensity ratio Hα/[NII] $\leq$ 1; see Table 2). According to Kaler 1978, such

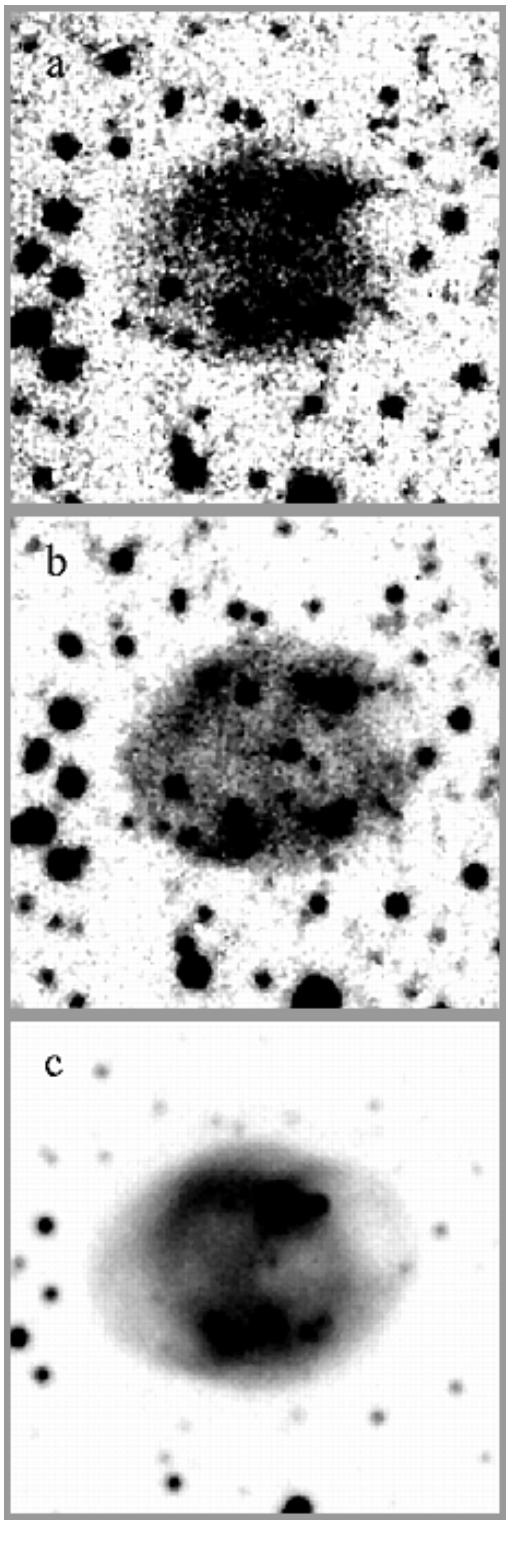

Fig. 1. A 60. **a)** Hα. **b)** [NII]. **c)** [OIII]. The bipolar structure of this elliptical planetary nebula is more conspicuous in [OIII]. Such a morphology resembles the bright core of He 2-119 and even the Dumbbell nebula (see below). In general, North is at the top, east towards the left for all figures unless otherwise noted

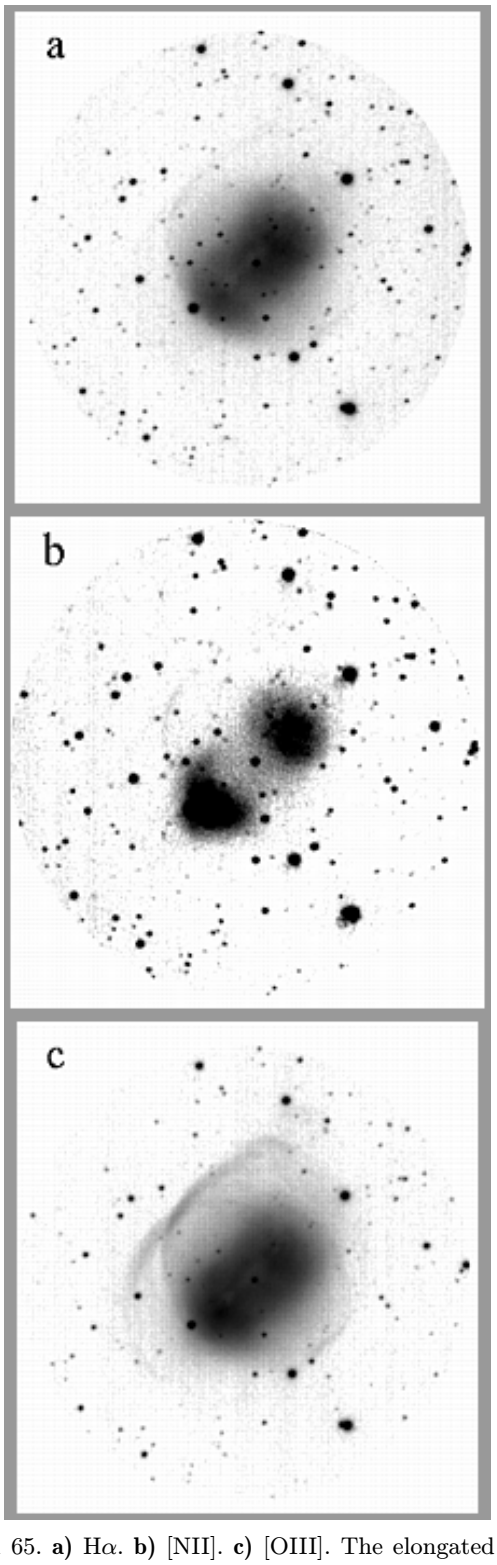

Fig. 2. A 65. **a)** Hα. **b)** [NII]. **c)** [OIII]. The elongated core is surrounded by a spectacular outer ring (double in [OIII]). The [NII] core is composed with two $60'' \times 60''$ blobs superimposed on a faint diffuse emission. The faint outer filament is still seen NE. Given such a structure, it is not surprising to "miss" the N^{++} lines, depending where the slit is placed! The [OIII] image displays almost the same structure as in Hα, but the outer filament shows up with a double ring much stronger

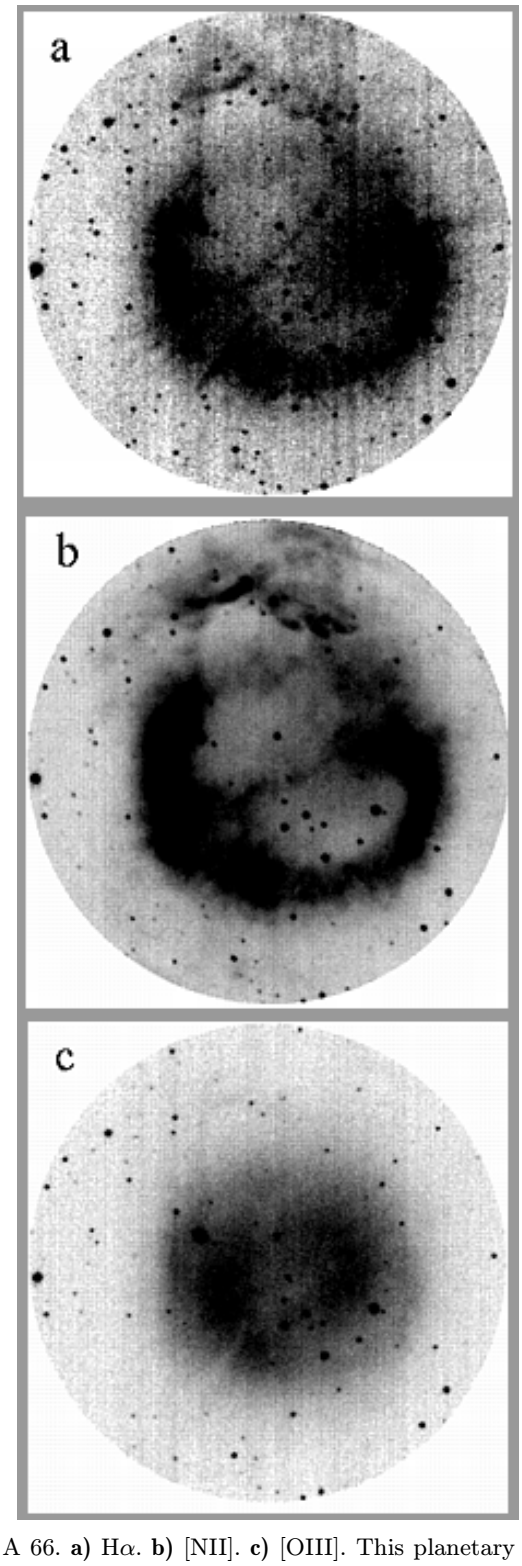

Fig. 3. A 66. **a)** Hα. **b)** [NII]. **c)** [OIII]. This planetary nebula resembles the "Owl Nebula". The Hα diameter measures 320″. The N filament displays a string of eastward condensations. The overall dimensions should be even larger than the actual field of view offered by the CCD (northward extension). The outer [NII]6583 emission is much more conspicuous than that seen in Hα which also displays helical strings (NW-SE) around the broken circular annulus. The outer emission detected in the two previous emission lines is no longer seen in the (smaller due to higher ionization potential) [OIII] image which shows a patchy line across the bright centre separated in two blobs. The two cavities seen in Hα and [NII] no longer exist here

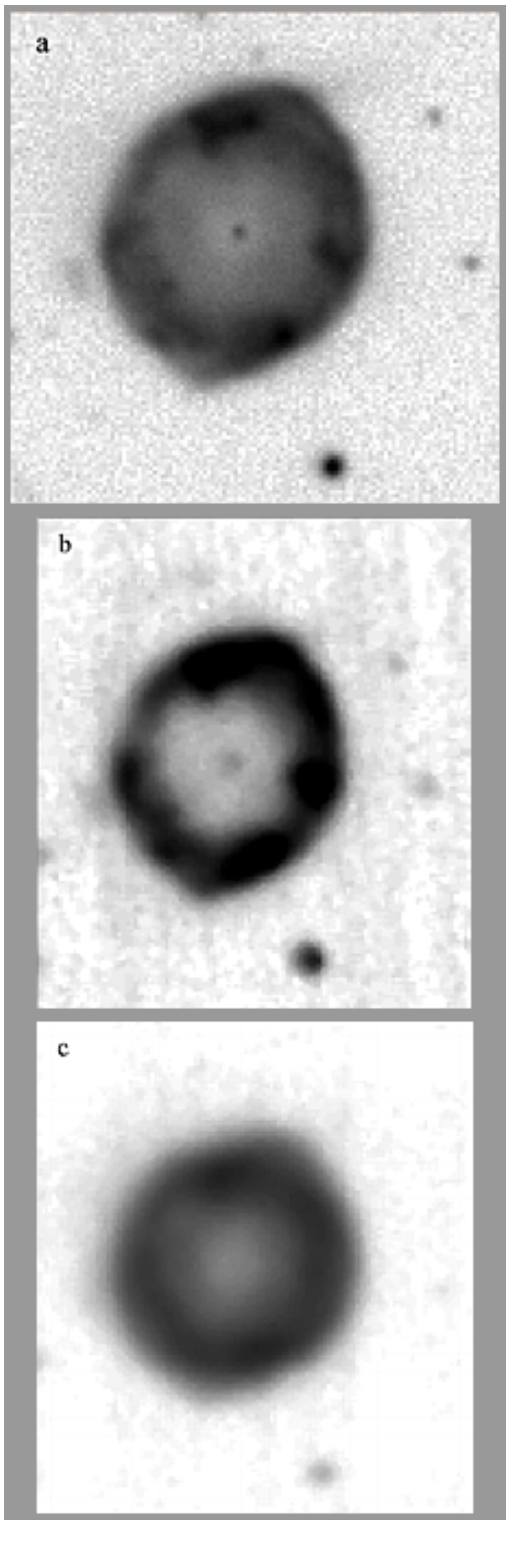

Fig. 4. A 70. **a)** Hα. **b)** [NII]. **c)** [OIII]. A faint NE emission is detected for this nearly circular (50″) planetary nebula. Its ring structure displays 6 bright knots. The [NII] and [OIII] condensations more obviously outline the circular ring (smaller ring in oxygen)

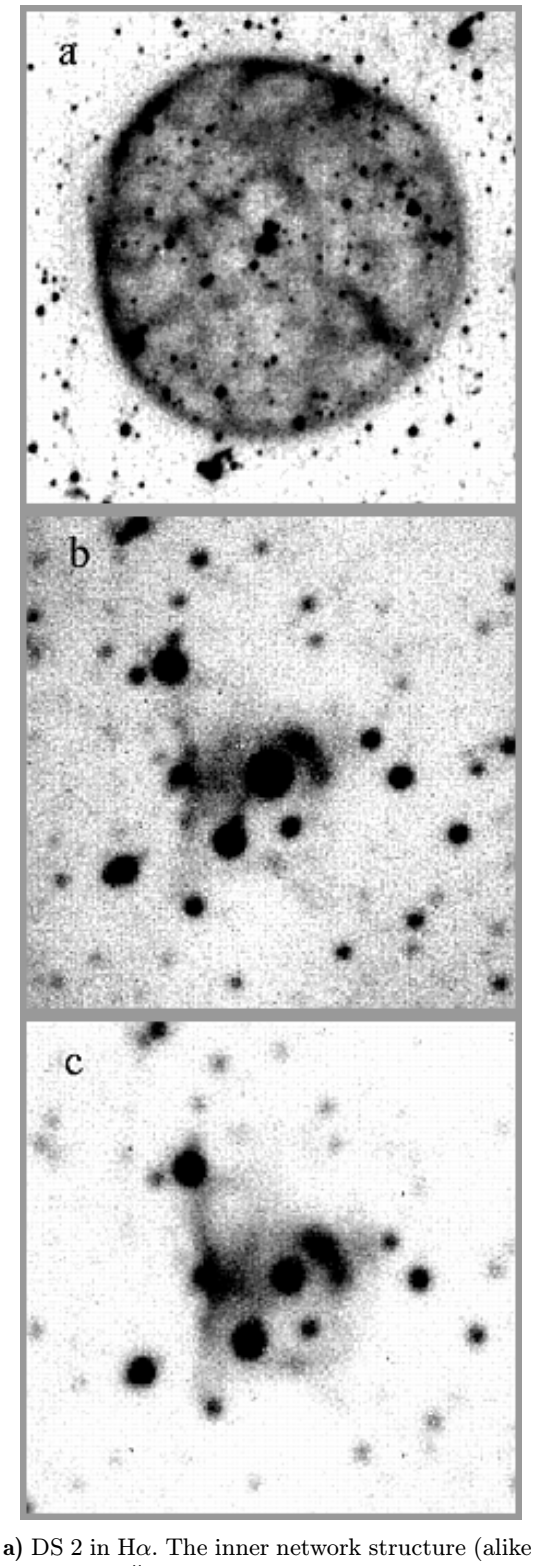

Fig. 5. a) DS 2 in Hα. The inner network structure (alike A 43) spreading over 190″ of the Hα image suggests Rayleigh-Taylor instabilities. [NII] and [OIII] emissions were not detected. **b)** DuRe 1 in Hα. The faint emission around a bright central star is a diffuse disk of 55″. **c)** DuRe 1 in [NII]: A faint NE filament is probably present in [NII]. [OIII] was not detected

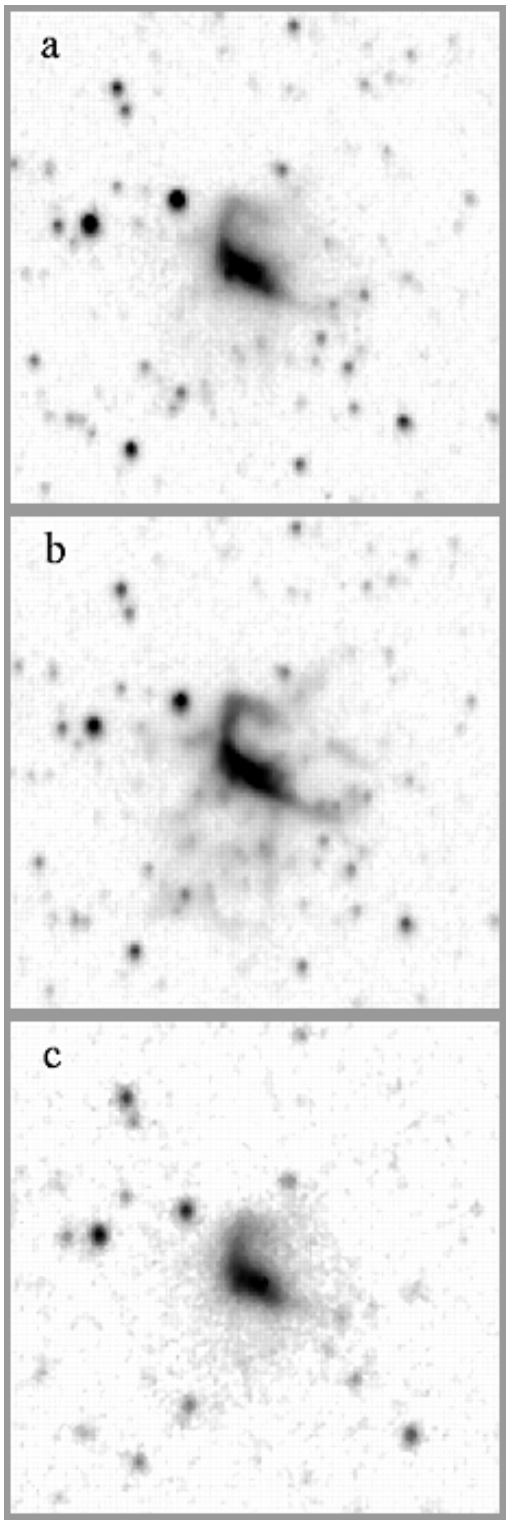

Fig. 6. He 2-70. **a)** Hα. **b)** [NII]. **c)** [OIII]. This planetary nebula also displays a "crab" or "spider"-structure. Nitrogen is much stronger than Hα and [OIII]

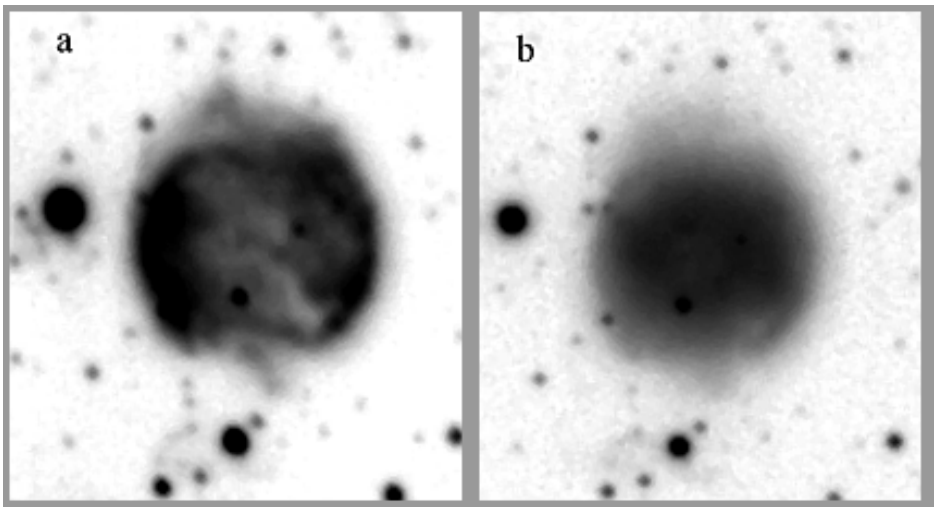

Fig. 7. He 2-72. **a)** [NII]: Two lobes provide the bipolar shape along the minor axis of a ring structure. Two ansae end the major axis (NS). **b)** The [OIII] image is smaller and rather circular

high-excitation class PNe would have low IRE and central star effective temperatures larger than 60 000 K (see Fig. 11, p. 78 in Zijlstra's thesis). Note the large discrepancies between optical and radio extinction values (Table 2) for the PNe of our sample.

These above selection criteria ensure that we have observed relatively nearby PNe, and which are mostly Peimbert Type I PNe. Such PNe presumably have relatively massive progenitors which have been through a third dredge-up stage with "hot-bottom burning" on the AGB, producing a relative overabundance of nitrogen. These more massive PNe lose a greater fraction of their mass while on the AGB, and have more and more frequent helium shell flashes. They are therefore better candidates to discover remnants of material ejected in previous helium shell-flash episodes. They are also characterized by more rapid evolution and more energetic stellar winds during the PN phase.

3. Results

In this section, comments are given for new detection of outer structures (if and where they exist) as observed through three interference filters (Hα, [NII]6583, and [OIII] 5007). We are interested here with the PN ionized mass estimates. PN distances and electron densities are principal sources of uncertainties. As a matter of fact, our present monochromatic survey shows that most PNe have angular diameters much larger than catalogued so far, which implies to revise values of the PN ionized mass, which is expressed by the formula:

$$M_{\rm ion} = \frac{\frac{4}{3}\pi r_{\rm cm}^3 \times \epsilon \times N({\rm H}^+) \times 1.4 \times 1.624\ 10^{-24}}{1.989\ 10^{33}}$$

where $r_{\rm cm}$ is the linear radius, ϵ the filling factor and $N({\rm H}^+) \sim N_{\rm e}$. In practice, we use distance determinations from CKS92 to determine $r_{\rm cm}$, and provide estimates of ionized mass as functions of $\epsilon \times N_{\rm e}$ (the numerical value represented by α is given in Table 2, Col. 11). When possible, we derive electron densities from Zhang (1988, thesis p. 76), but again, the accurate knowledge of distance is crucial here:

$$4.732 \times S_{6\ {\rm cm}}^{1/2} r_{''}^{-3/2} \epsilon^{-1/2} d_{\rm kpc}^{-1/2}.$$

Measured absolute fluxes for individual PNe are provided in Table 3. For the sake of clarity, only total fluxes are indicated in this table, detailed values for inner/outer regions are given in the text for the PN in question.

3.1. A 60 − PN G 025.0 − 11.6

The Hα ($75''\times65''$) and [NII]6583 Å ($90''\times80''$) emissions are rather faint as compared to the [OIII]5007 Å ($110''\times95''$) ones (Figs. 1). The latter shows a more evident bipolar structure inside the elliptical shape. The [NII] emission was not reported by spectroscopy (AST91 in Acker93). The global structure is far from homogeneous. At the distance of 1705 pc (CKS92), the [OIII]5007 major axis measures 0.91 pc. Using $S(6\ {\rm cm}) = 11\ 10^{-3}$ Jy and the theoretical relationship (see Pottasch 1984, p. 203) with $I({\rm H}\beta)$, we derive a rather high reddening $c({\rm H}\beta) = 1.477$, leading to $E(B-V) = 1.01$. The ionized mass computed with the Hα image radius $r_{\rm cm}(37''5)$ provides $M_{\rm i} = 4.35\ 10^{-3}$ $\epsilon\ N_{\rm e}$. With $N_{\rm e} \sim 95\ {\rm cm}^{-3}$, and assuming $\epsilon = 0.3$, the ionized mass amounts $\sim 0.12\ M_\odot$.[1]. The absolute flux measurements are given in Table 3.

[1] Electron density values derived with Zhang's formula are generally low.

3.2. A 65 − PN G 017.3 − 21.9

This PN is characterized by a relatively moderate IRAS emission (peak at 100 μm) and a rather low expansion velocity ($v_{[\mathrm{OIII}]} = 11$ km s^{-1}).

We have detected (Figs. 2) more extended structures (overall dimensions $270'' \times 250''$) than the $100''$ quoted so far (which do correspond to the dimensions of the main and bright rectangular core). As a matter of fact, the nebular core is surrounded by an elliptical diffuse emission, and a faint outer halo, in three emission lines. The rectangular centre consists of two conspicuous lobes, particularly more obvious in [NII] (this emission line was not reported by spectroscopy, see Acker93. Moreover, given such a structure, one can easily miss the [NII] emission, depending on how the slit is placed across the nebula!).

The Hα overall dimensions measure $270'' \times 250''$ (in Table 2 we give the inner area dimensions), while the [NII] dimensions are slightly smaller with $250'' \times 210''$ and [OIII] with $240'' \times 220''$ or 1.93 × 1.77 pc (at 1655 pc, CKS92, $1'' = 8.02\ 10^{-3}$ pc). The ionized mass of the inner ($r = 70''$) bright area amounts $2.60\ 10^{-2} \times \epsilon\ N_{\mathrm{e}}$. Assuming $N_{\mathrm{e}} = 100$ cm^{-3} and $\epsilon = 0.3$, we obtain $M_{\mathrm{i}} = 0.78\ M_{\odot}$. For the overall nebula ($r = 100''$) which would concern a less dense medium, we get $7.55\ 10^{-2} \times \epsilon\ N_{\mathrm{e}}$. If $N_{\mathrm{e}} = 50$ cm^{-3}, the overall ionized mass would be larger than 1 $M_{\odot}$. The outer halo in [OIII] suggests two large rings intersecting southwards. The comparison with the theoretical Hβ flux provides $c(\mathrm{H}\beta) = 0.241$ and $E(B-V) = 0.165$.

3.3. A 66 − PN G 019.8 − 23.7

This "old" planetary nebula was reported in Abell 1955 and 1966 and given a circular type with a $267''$ diameter (CaKa71). Our observations show the spectacular extension spreading over the $6'5$ field of view, definitely larger than quoted. The Hα image (Figs. 3) shows a NE filamentary structure attached to the main annulus, along with circular rings surrounding the central area. Radial structures escape outwards. These features are less obvious in the [NII]6583 Å, no longer seen in [OIII]5007 Å which displays strong bipolar E-W emission. Moreover, the [NII] dimensions appear much larger than that in Hα. At 567 pc, $1'' = 2.749\ 10^{-3}$ pc, the overall diameter ($320''$) of this nearby planetary nebula measures ~ 0.90 pc. The ionized mass of the inner spheroidal nebula ($260''$) amounts $6.67\ 10^{-3} \times \epsilon\ N_{\mathrm{e}}$, or 0.12 $M_{\odot}$, assuming $\epsilon = 0.3$ and $N_{\mathrm{e}} = 60$ cm^{-3}, whereas the overall planetary would have $12.44\ 10^{-3} \times \epsilon\ N_{\mathrm{e}}$. and assuming $\epsilon = 0.3$, the ionized mass amounts $\sim 0.12\ M_{\odot}$. The ratio inner/outer ionized mass is roughly 0.70, since we suspect the total dimensions of this PN would be even larger than our field of view. The [OIII]5007 image displays a spheroidal structure crossed by a dusty patch close to the centre. The previous NE "tail" seen in Hα and [NII] is no longer visible, probably too faint. The radio flux $S(6\ \mathrm{cm}) = 58$ mJy leads to $I(\mathrm{H}\alpha) = 45.4\ 10^{-13}$ erg cm^{-2}s^{-1}.

3.4. A 70 − PNG 038.1 − 25.4

The Hα image (Figs. 4) showing a prominent central star, displays condensations along the elliptical ring. A faint eastward emission is visible on the Hα and [NII] images. The overall diameter measures $50''$. The [OIII] is rather circular and $\sim 15\%$ smaller than the previous emission lines. The ionized mass with $r = 25''$ amounts $3.40\ 10^{-3} \times \epsilon \times N_{\mathrm{e}}$. Assuming $\epsilon = 0.3$, we compute $N_{\mathrm{e}} = 150$ cm^{-3}, and find $M_{\mathrm{i}} = 0.16\ M_{\odot}$.

3.5. DS 2 − PN G 335.5 + 12.4

This is probably the first monochromatic image (Fig. 5a) of DS 2 obtained since its discovery by Drilling in 1983. [NII]6583 and [OIII]5007 were not detected (nitrogen and oxygen probably absent). The Hα image with its $190''$ diameter suggests Rayleigh-Taylor instabilities. In absence of the distance's measurement, we were not able to derive its ionized mass.

3.6. DuRe 1 − PNG 302.3 − 01.3

The Hα image (Fig. 5b) shows a prominent central star. The [NII] (Fig. 5c) emission is more conspicuous with faint filament tied up westwards. As for DS 2, we cannot compute the ionized mass without knowledge of the PN distance.

3.7. He 2-70 − PNG 293.6 + 01.2

This planetary nebula, observed at MJUO, displays a $60''$ "crab" structure surrounded by a fuzzy emission (Figs. 6). The [NII] image is slightly more extended, and the [OIII] image is smaller than the two other emission lines. Using $d = 1900$ pc (Maciel 1984) we obtain $M_{\mathrm{i}} = 3.085\ 10^{-3}\ \epsilon\ N_{\mathrm{e}}$.

3.8. He 2-72 − PNG 294.9 − 00.6

This planetary nebula was observed only in [NII]6583 Å (Fig. 7a) and [OIII]5007 Å (Fig. 7b). Its distance is unknown, one cannot estimate the ionized mass.

Table 1. List of observed PNe

Names	$PNG_{Acker93}$	α(2000)	δ(2000)	12 μm	25 μm	60 μm	100 μm	S(6 cm)	$-\log F(H_\beta)$	d(pc)
1	2	3	4	5	6	7	8	9	10	11
A 60	025.0−11.6	19 19 17.5	−12 14 52	*	*	*	*	11	13.0	1705
A 65	017.3−21.9	19 46 33.8	−23 08 12	0.25	0.71	1.35	3.05	41	11.63	1655
A 66	019.8−23.7	19 57 31.8	−21 36 37	0.25	0.40	0.40	1.93	58	*	567
A 70	038.1−25.4	20 31 33.1	−07 05 21	*	*	*	*	12	12.34	2353
DS 2	335.5+12.4	15 43 00	−39 20 00	*	*	*	*	*	*	*
DuRe 1	302.3−01.3	12 45 51.2	−64 09 38	*	*	*	*	*	*	*
He 2-70	293.6+01.2	11 35 13	−60 16 54	0.25	0.45	1.70	35.0	*	12.2	1900*
He 2-72	294.9−00.6	11 41 38	−62 28 54	*	*	*	*	*	*	*
He 2-119	317.1−05.7	15 10 39.9	−64 40 19	0.59	1.52	8.79	9.83	94	11.8	1359
Hf 48	290.1−00.4	11 03 56	−60 36 06	*	*	*	*	*	12.7	2000*
IC 4406	319.6+15.7	14 22 26.5	−44 09 06	0.33	2.69	21.08	25.35	110	10.75	2358
IC 5148-50	002.7−52.4	21 59 30	−39 23 00	0.25	0.36	2.36	5.89	*	11.5	1058
K 1-3	346.9+12.4	16 23 17.3	−31 44 57	*	*	*	*	< 9	12.28	594
K 2-7	0.19.4−19.6	19 40 30	−20 27 00		*	*	*	*		1.27/2.6
Lo 17	356.8−11.7	18 27 48	−37 16 00	*	*	*	*	*	*	*
NGC 246	118.8−74.7	00 47 03.8	−11 52 22	0.25	2.43	9.11	19.24	248	10.53	470
NGC 3699	292.6+01.2	11 27 59.2	−59 57 32	0.31	4.21	6.88	10.08	67	11.22	1605
NGC 5189	307.2−03.4	13 33 42	−65 58 30	1.26	13.47	33.73	31.29	507	10.52	540
NGC 6302	349.5+01.0	17 13 44.3	−37 06 06	32.08	335.90	849.70	537.40	3034	10.55	525
NGC 6853	060.8−03.6	19 59 36.2	+22 43 01	0.45	3.13	19.79	58.40	1325	9.46	262
SaWe 3	013.8−02.8	18 26 03.1	−18 12 06	*	*	*	*	*	12.3	*
SaWe 4	014.7−11.8	19 02 16.1	−21 26 51	*	*	*	*	*	12.6	*

S(6 cm) in mJy. Distance values marked by (*) were taken from Maciel 1984. Size's values (Col. 11) and some other parameters are mainly taken from Acker93.

3.9. He 2-119 − PNG 317.1 − 05.7

A large circular halo (diameter $\sim 215''$) was detected around the $53''$ core. Rather faint in Hα, much stronger in [NII] and diffuse in [OIII], this explosive structure (Figs. 8) could be the remnant of the early ejections of stellar material. The spheroidal envelope resembles the overall appearance of NGC 6543 (Hua 1997). The absolute calibration is quite difficult (see below for SaWe 3 for instance), due to the presence of number of stars in the field. The values given in Table 3 are estimated within 20% uncertainty. For the inner elliptical area (80×120) $F_{\rm i}$(Hα) = 1.47 10^{-11} erg cm^{-2} s^{-1}; $F_{\rm i}$([NII]) = 3.1 10^{-11} erg cm^{-2} s^{-1}; $F_{\rm i}$([OIII]) = 5.87 10^{-11} erg cm^{-2} s^{-1}. In Table 3 we give flux values including the halo for three filters. When subtracting the central nebula and stellar contributions, one obtains an upper limit of 3 10^{-12} erg cm^{-2} s^{-1} for the faint halo. For [NII], $F_{\rm h}$([NII]) = 3. 10^{-11} erg cm^{-2} s^{-1}. For oxygen, $F_{\rm h}$([OIII]) = 7.6 10^{-12} erg cm^{-2} s^{-1}. Using the Hα diameter ($215''$), the ionized mass is equal to 5.19 $10^{-2} \times \epsilon \times N_{\rm e}$, leading to $M_{\rm i} \sim 1\ M_\odot$ if $\epsilon = 0.3$ and $N_{\rm e} = 65$ cm^{-3}.

3.10. Hf 48 − PN G 290.1 − 00.4

This planetary nebula is characterized by a quite strong reddening, since the Balmer decrement is rather high (10.17), and by a strong [NII] emission. The major part consists of a rectangular ($10'' \times 15''$) core. The fuzzy ($20'' \times 25''$) envelope is very faint. The surrounding fuzz (Figs. 9) emits a flux $\sim 2\ 10^{-13}$ erg cm^{-2} s^{-1}. In nitrogen, the central area has the same dimensions (2.94 10^{-12} erg cm^{-2} s^{-1}) but the outer extensions are larger. The surrounding fuzz then emits a flux $\sim 1\ 10^{-13}$ erg cm^{-2} s^{-1}. In [OIII] (2.2 10^{-12} erg cm^{-2} s^{-1} for the centre), 1.10^{-12} erg cm^{-2} s^{-1} are due to the surrounding envelope. At the distance of 2000 pc (Maciel 1984), $1'' = 2.99\ 10^{16}$ cm, the nebular radius ($12''5$) measures 3.74 10^{17} cm. One obtains for the ionized mass 2.5 $10^{-4} \times \epsilon \times N_{\rm e}$ which could amount roughly $\leq 0.1\ M_\odot$, if $\epsilon = 0.3$ and $N_{\rm e} = 1000$.

3.11. IC 4406 − PN 319.6 + 15.7

What is the real structure of the PN IC 4406? Discovered almost a hundred years ago (Stewart 1898), this PN shows low and high ionization species. The narrow-band filter photographs (Warner 1974) display the bright central bulk in [OIII]5007, Hα, [NII]6583, [OI]6300 and [SII]6717−6731 as well, with this remark that *the central region does not appear to be completely filled in* (Warner 1974). Its apparent "cigar-shape" resembles NGC 6905. The outer emission was reported as due to low ionization potential ions ([SII], [NII] and [OI]). Nonetheless, spectroscopic data

Table 2. Parameters of observed PNe

Names	Hα	[NII]	[OIII]	He/H	C_α	$C_{\rm radio}$	$\rm Size_{H\alpha}$	$\rm Size_{[NII]}$	$\rm Size_{[OIII]}$	α	Flux density	
1	2	3	4	5	6	7	8	9	10	$\times 10^3$	S(6 cm)*	$-\log F(\rm H_{beta})$*
A 60	454	-	969	0.110			75 ×65	90 ×80	110 ×95	4.35	0.53	14.32
A 65	231	-	318	0.110	0.19	-0.32	190 ×215	110 ×190	185 ×210	75.5	1.85	12.98
A 66	100	78	248	0.110			320	320	215	6.67	<< 1	*
A 70	300	553	804	0.110	0.07	0.90	50	50	50	3.39	1.09	13.38
DS 2	new						190	ND	ND	*	*	*
DuRe 1	new						55	55	ND	*	*	*
He 2-70	705	4043	1303				60	65 ×75	60	3.09	*	13.42
He 2-72	674	1045	920					75 ×80	75 ×80			
He 2-119	452	492	848	0.110			215	280	240	51.94	2.85	13.32
Hf 48	1017	6083	1353				25 ×20	28 ×80	20 ×65	0.26	*	13.88
IC 4406	390	595	1267	0.141	0.28	0.27	120	125	125	51.24	1.01	11.79
IC 5148-50	169	79	410	0.138			135	135	135	6.54	*	13.24
K 1-3	100	4280	-	0.125	2.78		120 ×160	120 ×160	125	1.86	0.05	14.52
K 2-7							150				*	*
Lo 17	100	-	468				110	110	110-115		*	*
NGC 246	228	-	549	0.115	0.12	0.22	265	ND	230 ×280	4.08	0.90	12.97
NGC 3699	452	869	1790	0.110	0.64	0.39	145	175×255	175 ×255	2.63	2.84	12.59
NGC 5189	350	366	1428	0.110	0.85	1.83	140 ×195	140 ×195	140 ×195	5.3	2.43	12.84
NGC 6302	704	1758	1354	0.182	1.26	1.39	60 ×290	60 ×290	60 ×185	8.82	13.75	12.89
NGC 6853	262	255	1106	0.110	0.18	0.04	720	720	720	3.89	1.50	12.41
SaWe 3	650	3780	393				75 ×100	75 ×175	55 ×75		*	*
SaWe 4	400	-	400				50				*	*

He/H and extinction values are from CKS92. Flux density values are computed with the radio flux S(6 cm) in mJy from Table 1 and using the formula $S(6\ \rm cm) \times (d_{kpc}/7.8)^2$, and $F(\rm H\beta) \times (d_{kpc}/7.8)^2$. ND = not detected. The dimensions (for inner areas) in three emission lines are in arcseconds as measured in this report. Column 11 gives α's values to be multiplied by appropriate ϵ and $N_{\rm e}$ to obtain estimates of ionized mass in solar masses for the overall nebula (see text).

giving [OIII]5007/Hβ = 12.67 clearly demonstrate that IC 4406 belongs to the high excitation class (Acker93).

As a matter of fact, our monochromatic Hα and [OIII] images (obtained first at MJUO then at SSO) show (Figs. 10) condensations in the central area, separated by a north-south absorbing lane, whereas the outer extension spreads even farther than the western star, as seen in low-ionization transition by Warner 1974. In fact, its looks like a broken ring rather than a dense concentration towards the centre. Therefore, our observations do not agree with the Warner's geometry, since we notice three superposed structures. This result evidences the nonuniform distribution of matter in the very centre of the PN. The central area is formed with a bright centre crossed by an absorbing lane. In addition, a peculiar feature is present in [NII] and not seen in the two other lines (see Figs. 10). The absolute calibration is quite satisfactory between the data obtained first at MJUO and later at SSO, and provides for the for the bright centre $F(\rm H\alpha) = 4.35\ 10^{-11}$ erg cm^{-2} s^{-1}. Table 3 gives total fluxes emitted by the whole bright rectangle of $105'' \times 35''$. The ionized mass estimated with the overall Hα diameter ($120''$) equals $5.12\ 10^{-2} \times \epsilon \times N_{\rm e}$, or 1.9 $M_\odot$ assuming $\epsilon = 0.3$ and $N_{\rm e} = 125$.

Table 3. Absolute Fluxes for 22 PNe

Names	PNG	$F(\rm H\alpha)$	F([NII])	F([OIII])	$M_{\rm ionized}$
1	2	3	4	5	6
A 60	025.0−11.6	2.41	2.80	54.59	0.12
A 65	017.3−21.9	102.9	16.2	285.	0.78 to > 1
A 66	019.8−23.7	96.64	12.51	154.8	0.12
A 70	038.1−25.4	13.19	12.97	77.84	0.16
DS 2	335.5+12.4	27.92			
DuRe 1	302.3−01.3	18.72	107.6		
He 2-70	293.6+01.2	49.91	103.	19.7	∼ 1.
He 2-72	294.9−00.6		54.07	106.	
He 2-119	317.1−05.7	177.5	688.	660.	∼ 1.
Hf 48	290.1−00.4		39.4	33.	≤ 0.1
IC 4406	319.6+15.7	551.56	800.90	1335.26	1.9
IC 5148-50	002.7−52.4	247.	56.3	279.	≤ 0.2
K 1-3	346.9+12.4	9.61	76.6	16.8	0.058
K 2-7	019.4−19.6	12.2			0.04 to 3.6
Lo 17	356.8−11.7	31.	9.87	134.	
NGC 246	118.8−74.7	680.		1760.	0.16
NGC 3699	292.6+01.2	102.	250.	1390.	0.7
NGC 5189	307.2−03.4	593.	1200.	506.	1.5
NGC 6302	349.5+01.0	1770	4640	3930	
NGC 6853	060.8−03.6	*	*	*	1.16
SaWe 3	013.8−02.8	34.4	120.	23.3	
SaWe 4	014.7−11.8	4.44			

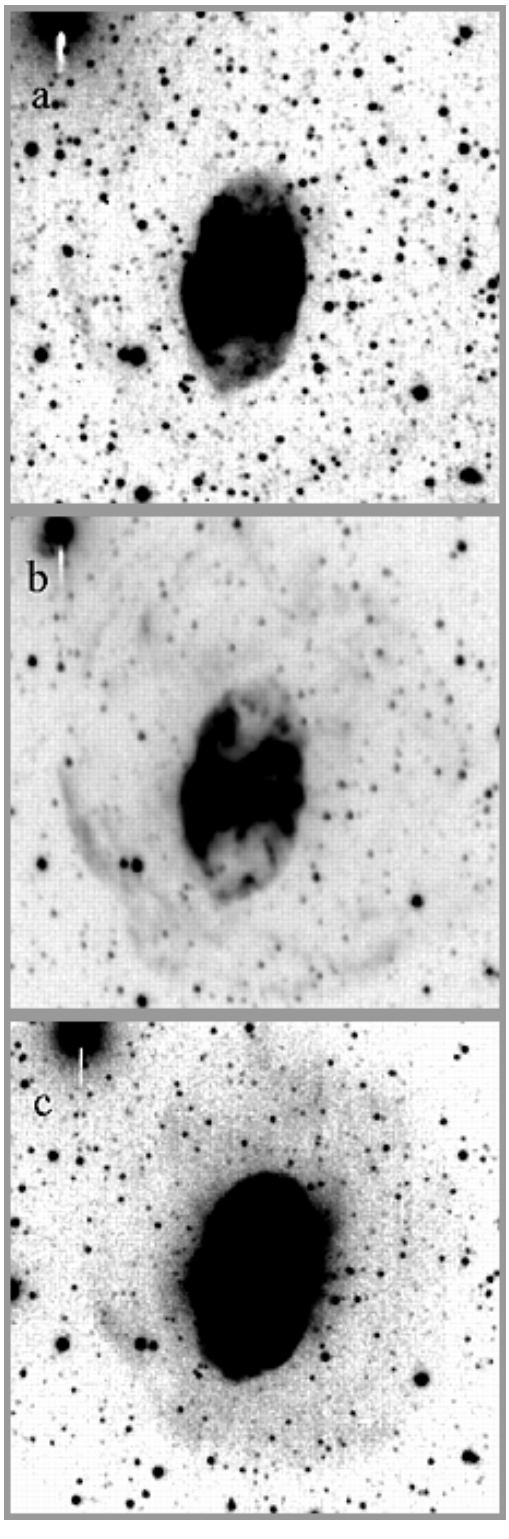

Fig. 8. He 2-119. **a)** Hα. **b)** [NII]. **c)** [OIII]. The outer big halo is more prominent in [NII] and [OIII] than in Hα. Radial structures are present around the inner [NII] core. The [OIII] outer halo is more diffuse

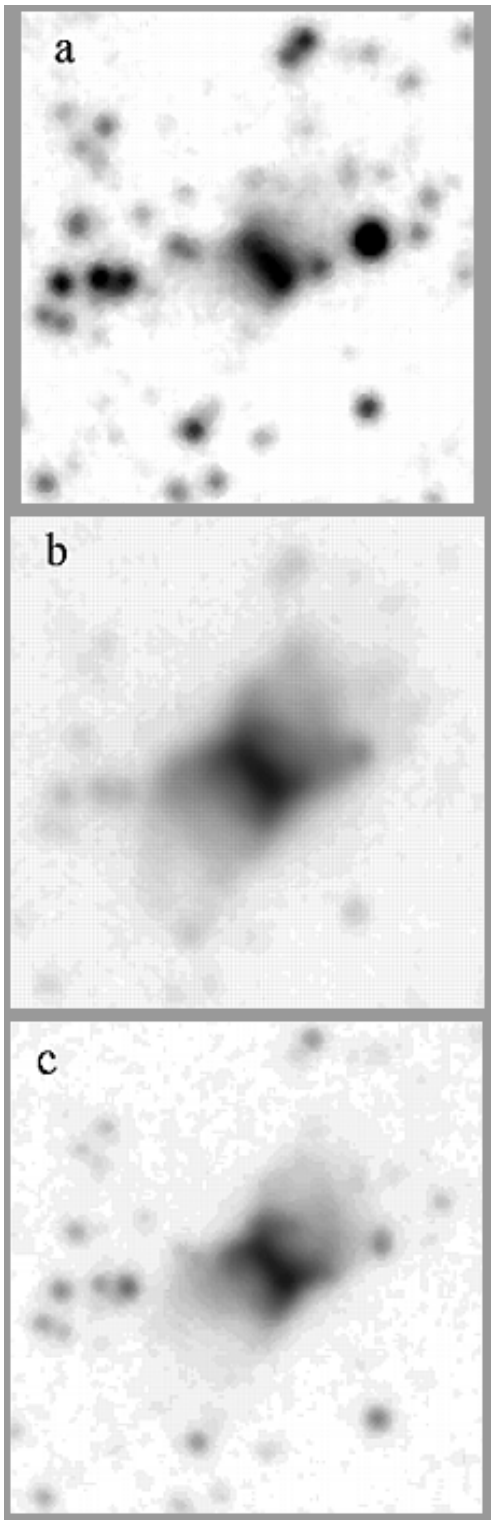

Fig. 9. Hf 48. **a)** Hα. **b)** [NII]. **c)** [OIII]. The rectangular core is seen in three wavelengths, with east-west emissions, more extended in [NII] and [OIII]

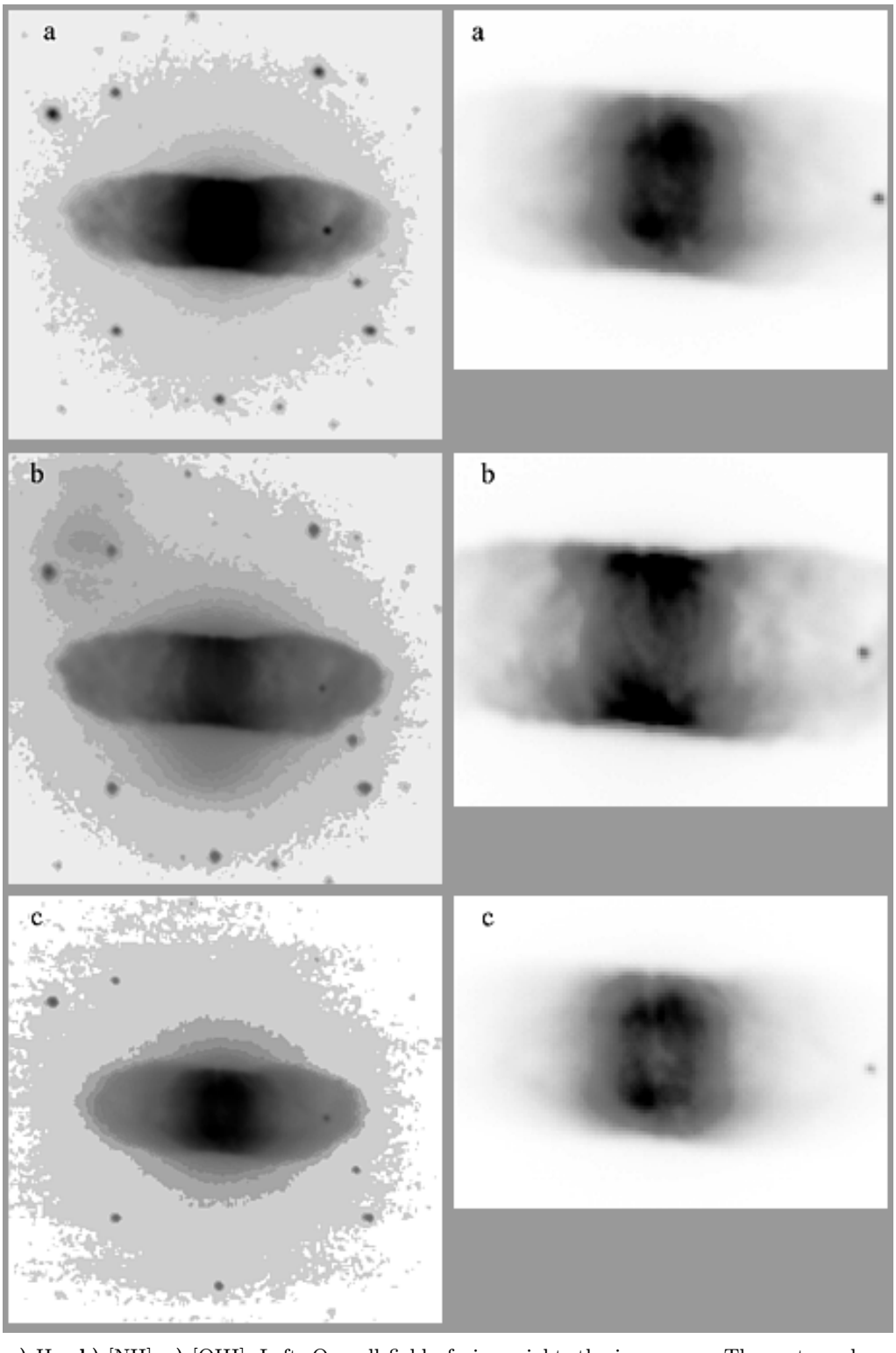

Fig. 10. IC 4406. **a)** Hα. **b)** [NII]. **c)** [OIII]. Left: Overall field of view; right: the inner core. The rectangular and bright inner core is surrounded by a $\sim 120''$ circular faint halo. The inner core in [NII] shows a different structure even though the EW dusty patch is still present. The rather prominent NE feature seen in [NII] was not detected in the two other filters. We initially attributed it to the "ghost" image due to the bright centre. However, after careful examination of the previous images taken at MJUO, with the Mc-Lellan 1 metre telescope, this emission nebulosity may be real. [OIII] displays the same structure as for Hα

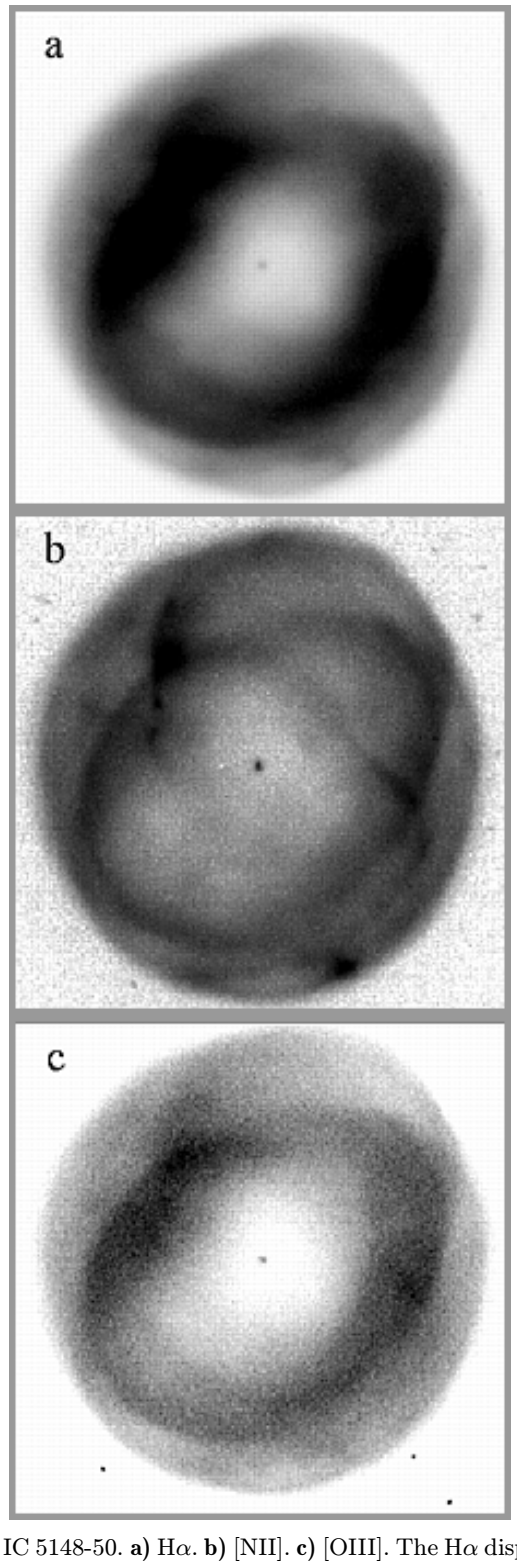

Fig. 11. IC 5148-50. **a)** Hα. **b)** [NII]. **c)** [OIII]. The Hα displays a multiple-shell structure with a bright inner ring. The [NII] image is marked by a mulptiple-ring and helical structure. [OIII] shows almost the same morphology as for Hα. The major axis is oriented NS (North at the up right corner)

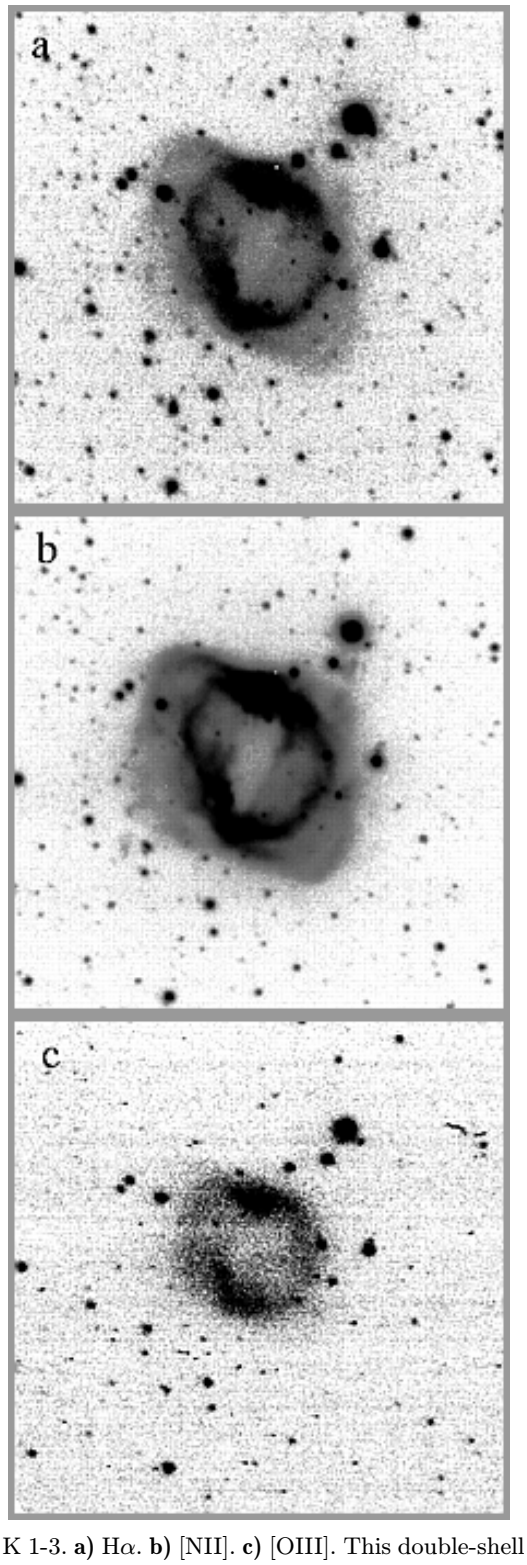

Fig. 12. K 1-3. **a)** Hα. **b)** [NII]. **c)** [OIII]. This double-shell planetary nebula displays a "shark-jaws" structure. The major axis is along the E-W direction. Two N-S blobs end the minor axis. Nitrogen is much stronger. Only the two inner peaks are seen superimposed on a diffuse and smaller emission in [OIII]. North at the up right corner

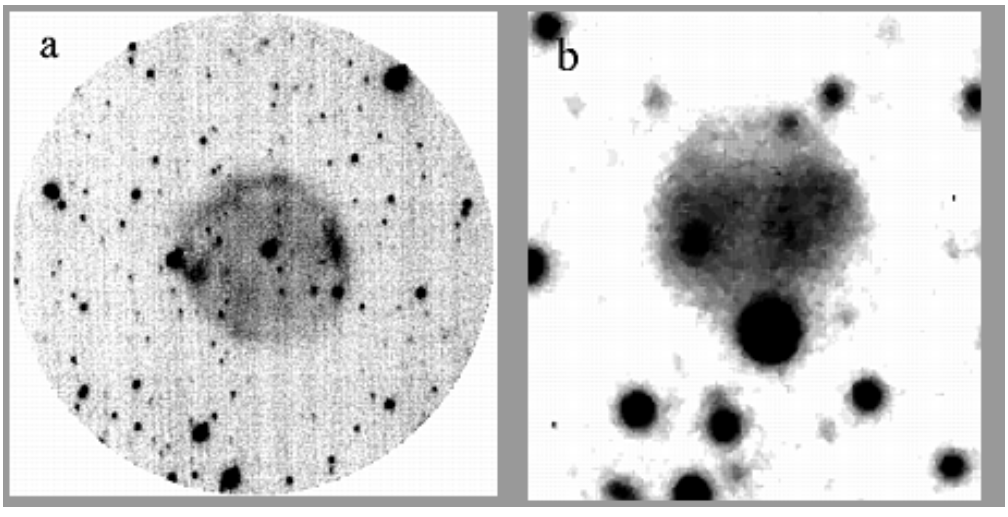

Fig. 13. a) K 2-7. Only the Hα image was obtained for this almost perfectly circular and faint planetary nebula. **b)** SaWe 4. Only the Hα image was obtained showing a circular shape

3.12. IC 5148 − 50 − PNG 002.7 − 52.4

Already observed at MJUO, this planetary nebula was reimaged at SSO. No new structure was detected in the present larger field of view (Figs. 11). The PN displays a double ring structure with 135″ diameter. The ionized mass amounts 6.54 $10^{-3} \times \epsilon \times N_{\rm e}$, or $\leq 0.2\ M_{\odot}$ assuming $\epsilon = 0.3$ and $N_{\rm e} = 100$.

3.13. K 1-3 − PNG 346.9 + 12.4

The overall dimensions (120″ × 160″) are larger than the 92″ quoted (Figs. 12). On underexposed image, only the bright inner (broken) ring would show up, giving K 1-3 a bipolar structure shape. But deep exposures reveal outer emissions. Oxygen is restricted in a circular shape with smaller dimensions. The ionized mass for a 160″ diameter amounts 1.86 $10^{-3} \times \epsilon \times N_{\rm e}$, or $0.058\ M_{\odot}$ with $\epsilon = 0.3$ and $N_{\rm e} = 100$.

3.14. K 2-7 − PN G 019.4 − 19.6

Surprisingly, few measurements were done on this PN since its discovery by Kohoutek on 1963. We could only observe the planetary nebula with the Hα filter (Fig. 13a) just before the clouds came in. Two distance measurements are available but with a factor 2 of discrepancy: from 1.27 kpc (Cahn & Kaler 1971) to 2.6 kpc (Maciel 1984). Therefore its ionized mass would amount 1.4 $10^{-2} \times \epsilon \times N_{\rm e}$ and $0.12 \times \epsilon \times N_{\rm e}$ respectively. Assuming $\epsilon = 0.3$ and $N_{\rm e} = 100$, one obtains $0.04\ M_{\odot}$ and ... $3.6\ M_{\odot}$!

3.15. Lo 17 − PN G 356.8 − 11.7

The Hα and [NII] (2400s integration) images which were first acquired at MJUO (1993), then completed with [OIII] (600s) at SSO (1997), display a "donut" shape (Figs. 14), with the overall diameter of 110″. The ionized mass could not be computed without knowledge of the distance. Its circular annulus shape resembles A 39.

3.16. NGC 246 − PNG 118.8 − 74.7

This high-excitation PN shows no [NII] emission. Three monochromatic images were obtained: Hα (Figs. 15), [OIII] and HeII much smaller and fainter. With 265″ diameter, its ionized mass equals 4.08 $10^{-3} \times \epsilon \times N_{\rm e}$, or $0.16\ M_{\odot}$ with $\epsilon = 0.3$ and $N_{\rm e} = 150$.

3.17. NGC 3699 − PNG 292.6 + 01.2

The Hα image (Figs. 16) of this planetary nebula displays a $\sim 145''$ dimension, leading to $M_{\rm i} = 2.63\ 10^{-3} \times \epsilon \times N_{\rm e}$, i.e. $\sim 0.7\ M_{\odot}$, assuming $\epsilon = 0.3$ and $N_{\rm e} = 100$. The [NII] image shows a spectacular extension which would be larger than our field of view (6′5). In addition, we have detected a faint emission nebula 50″ west of NGC 3699. For nitrogen, the computations of absolute flux were more difficult due to the overall extensions. Nevertheless, we obtain $F([\mathrm{NII}]) = 2.5\ 10^{-11}$ erg cm^{-2} s^{-1} for the main nebula, while the newly detected nebulosity emits $F([\mathrm{NII}]) = 8\ 10^{-13}$ erg cm^{-2} s^{-1}. In [OIII] (Fig. 16c) we get $F([\mathrm{OIII}]) = 5.21\ 10^{-13}$ erg cm^{-2} s^{-1} for the new object. The overall fluxes are given in Table 3.

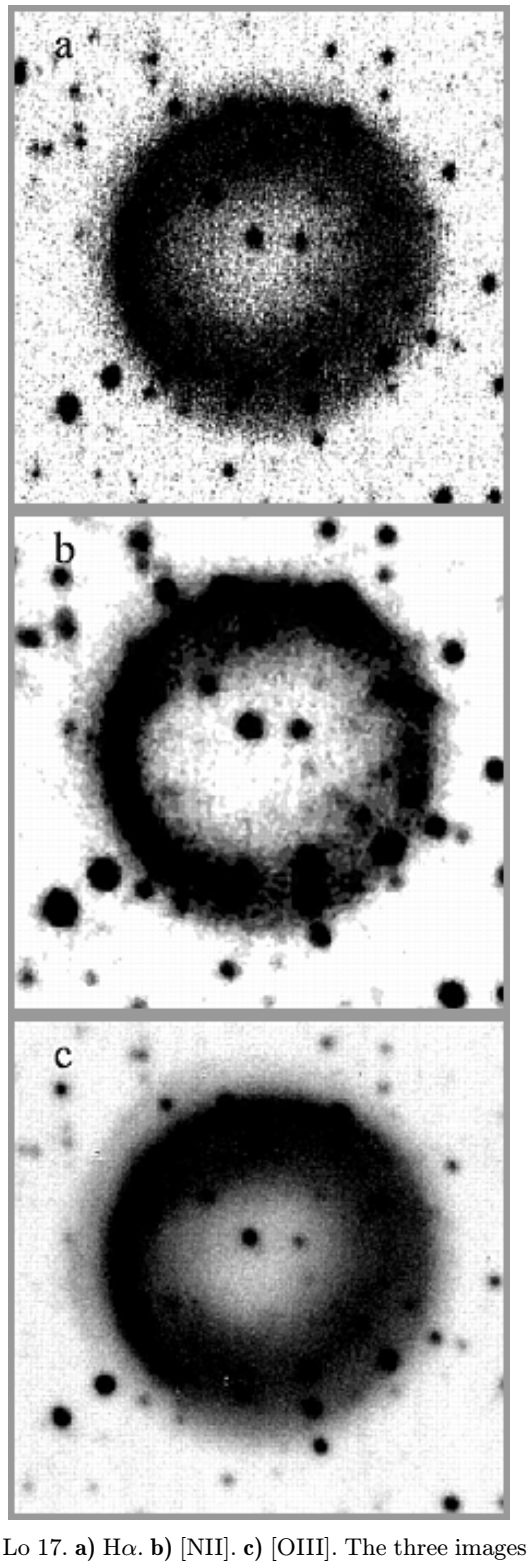

Fig. 14. Lo 17. **a)** Hα. **b)** [NII]. **c)** [OIII]. The three images show a nearly perfect circular ring, with probably an outer diffuse shell

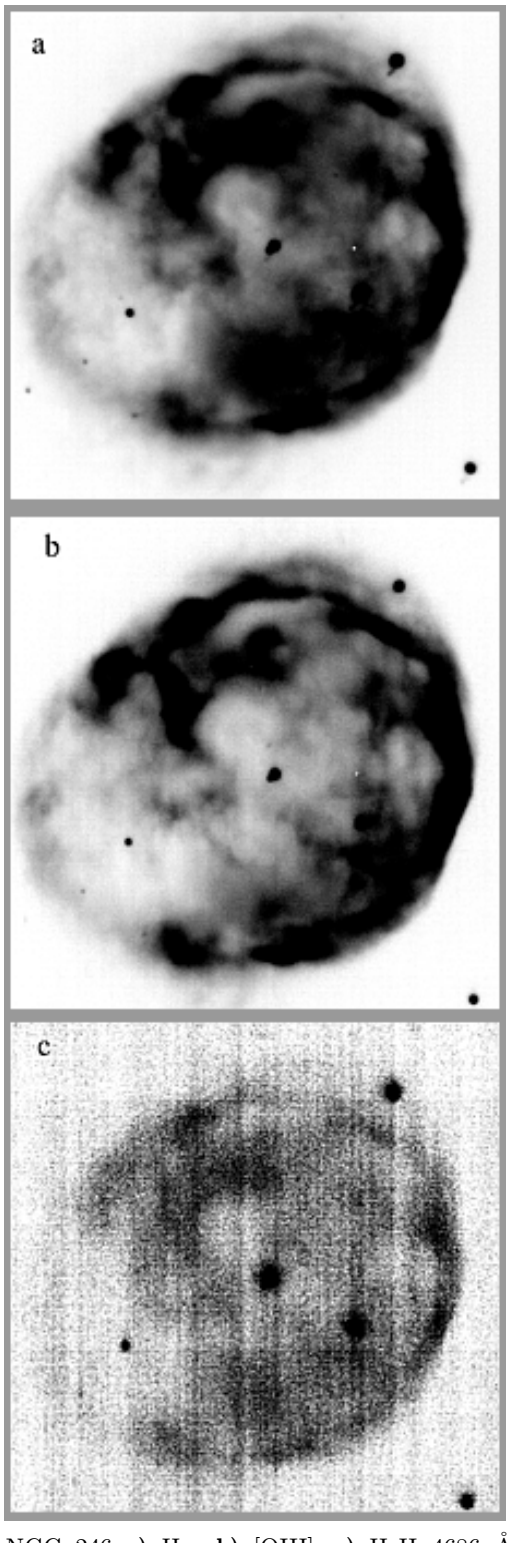

Fig. 15. NGC 246 **a)** Hα. **b)** [OIII]. **c)** HeII 4686 Å. This high-excitation PN has a similar structure in Hα and [OIII]. Nitrogen was not detected. HeIIλ4686 shows up very weak and has almost the same volume

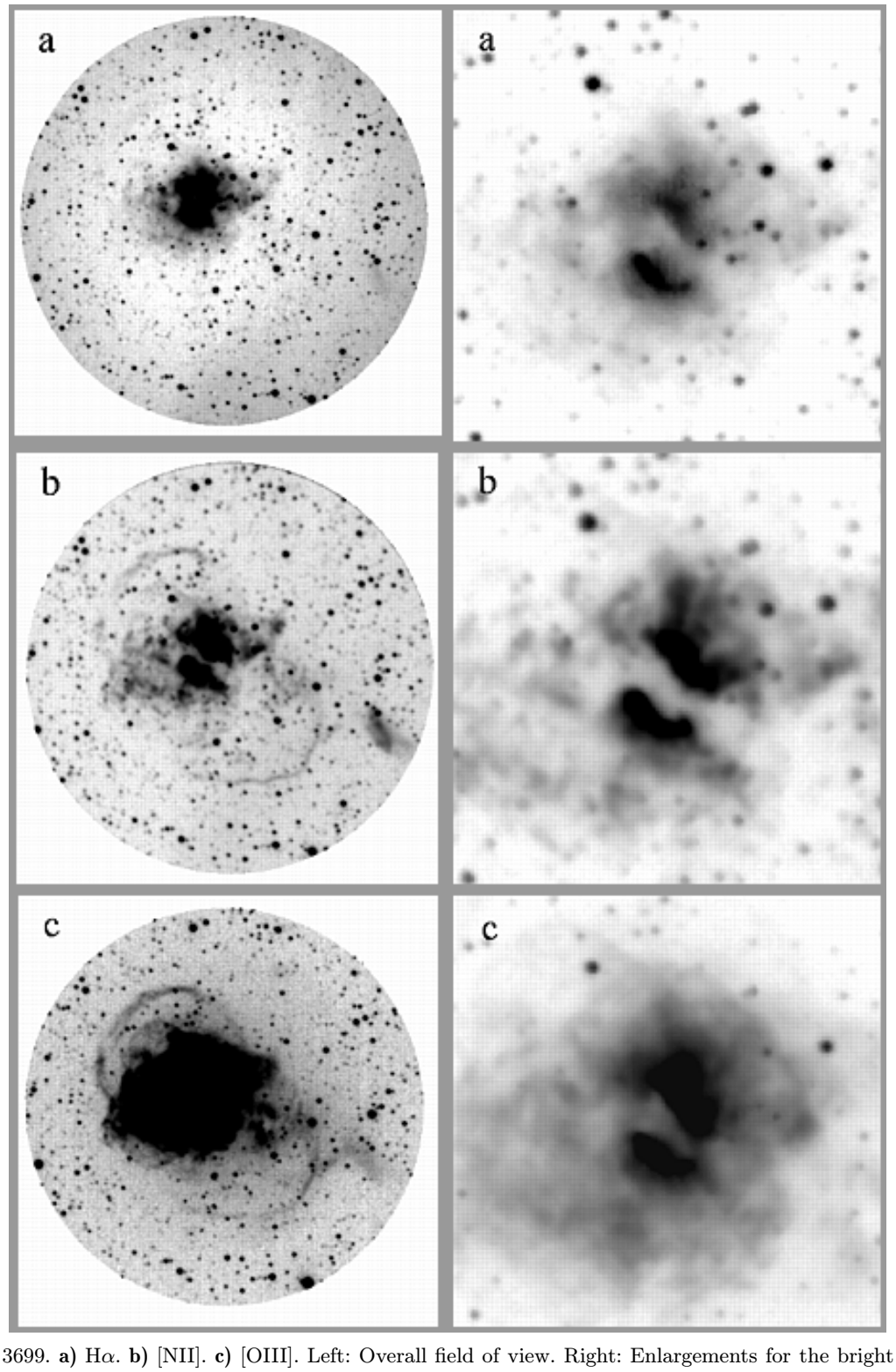

Fig. 16. NGC 3699. **a)** Hα. **b)** [NII]. **c)** [OIII]. Left: Overall field of view. Right: Enlargements for the bright central area. The two-lobe structure in the central area is probably due to a strong absorbing lane nearly oriented E-W, and superimposed on a fainter underlying emission. The nitrogen emission is much more prominent and much more extended than the two other emission lines. Notice a bright emission nebula at the W-side in the total field of view, still much brighter in [NII]. A faint and large loop spreads over $\sim$6 arcmin, in three wavelengths

3.18. NGC 5189 – PN G 307.2 – 03.4

Strong IRAS emissions were reported 12/25/60/100 = 1.26/13.47/33.73/31.29 as well as strong S(6 cm). The [SII] intensity ratio would imply $N_e \approx 10^3$ cm^{-3}. The largest dimension (Figs. 17) in the Hα image (195″) leads to the ionized mass 5.3 $10^{-3} \times \epsilon \times N_e$, or 1.5 $M_\odot$ if ϵ = 0.3 and the above electron density.

3.19. NGC 6302 – PNG 349.5 + 01.0

This PN was already observed at MJUO (Hua 1997). New monochromatic images (Figs. 18 & 19) were again performed at SSO through four filters Hα, Hβ, [NII]6583 Å, [OIII]5007 Å, and [SII]6717/6731 with the AAT 2.3-m telescope confirming an explosive structure surrounding a compact central core divided into two areas by an absorbing lane. The central area is much more brighter than the peripheral zones. Thanks to the larger field of view at SSO, we were able to outline the outermost extensions. The Hα and [OIII]5007 images have similar structures, whereas the [NII]6583 image displays condensations, and possibly the presence of a surrounding halo.

Presumably young (OH 1612 MHz detection by Payne et al. 1988), and due to its location near the galactic plane, this bipolar PN is strongly affected by high interstellar absorption since $E(B-V) = 0.93$ from the flux(radio)/flux(Hβ)ratio. The "strong physical condition": excitation class 10^+, the helium abundance He/H being twice (0,182) the average value for known PNe, are certainly related to the (invisible) central star with $B \geq$ 21.1, Acker93) the Stoy temperature of which is about 3 10^5 K, and even higher, up to 4.3 10^5 K (Ashley & Hyland 1988). Furthermore, nitrogen N/H (85 10^{-5}) is 10 times the average value (CKS92 and Pottasch 1984). Fast motions were detected in the [NeV]3426 Å line profile (Meaburn & Walsh 1980) with velocities approaching 800 km s^{-1}.

This very dusty PN with strong IRAS data 12/25/60/100 = 32.08/335.90/849.70/537.40 and S(6 cm) = 3100 mJy shows an outstanding "butterfly" morphology. In addition, it is overabundant in nitrogen (Hα/[NII]/[OIII] = 704/1758/1354). The [SII] intensity ratio (64/99) implies a high electron density. As a matter of fact, our narrowband images clearly demonstrate that this parameter is far from uniform across the nebula. The plot of the intensity ratio [SII]6717/6731 (Fig. 18d) shows the variation of N_e, from $\sim 10^4$ cm^{-3} in the very bright centre (in white; the [SII]6717/6731 ratio is ≤ 0.5) to a few hundreds cm^{-3} (in black; [SII]6717/6731 $\sim$ 1.2).

The absolute calibration gives for the bright rectangular area F_1(Hα) = 1.71 10^{-10} erg cm^{-2} s^{-1}. This determination is in very good agreement with that (2.10 10^{-10} erg cm^{-2} s^{-1}) reported by Hua 1997, considering the fact one cannot adjust quite exactly the integration contour

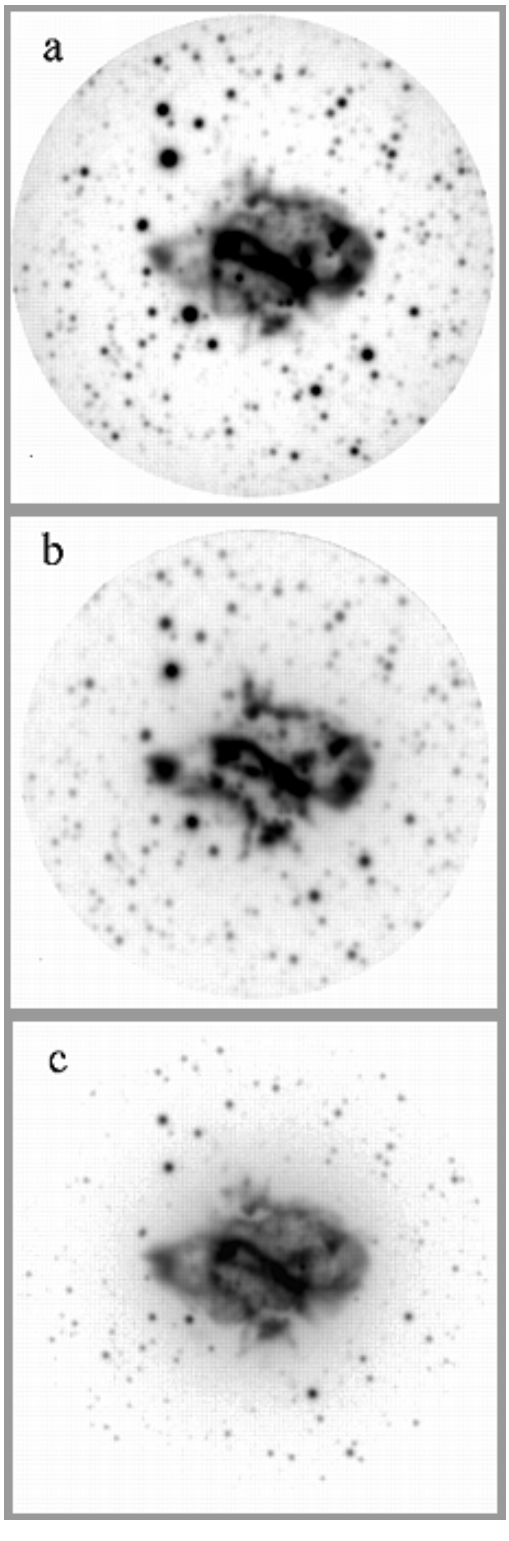

Fig. 17. NGC 5189. **a)** Hα. **b)** [NII]. **c)** [OIII]. This "Z-shape" already observed at MJUO is confirmed with SSO's images for this planetary nebula which displays a strong filamentary structure

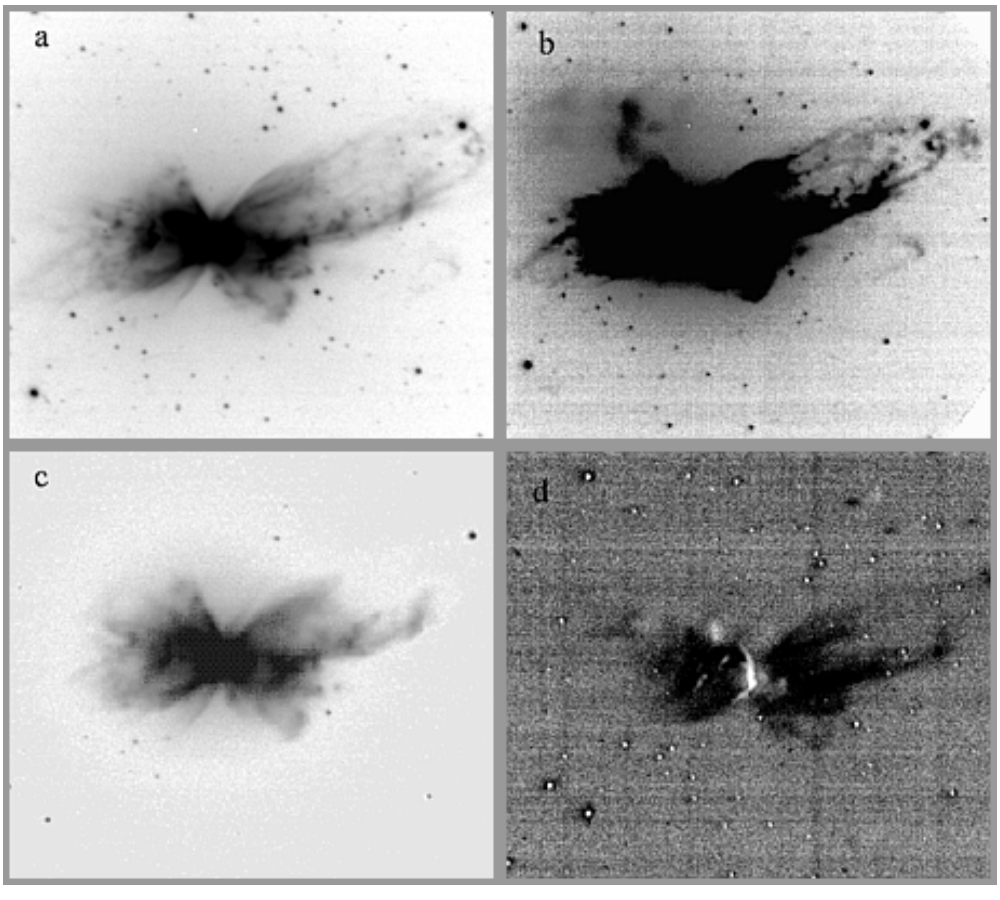

Fig. 18. NGC 6302. **a)** Hα. **b)** [NII]. **c)** [OIII]. **d)** The [SII]6717/6731 intensity ratio. The remarkable "butterfly-shape" appears in three emission lines, but more extended in [NII]. The electron density is rather high in the very centre which is seen in white, whereas the outer area corresponds to $N_e < 10^3$

around the nebula. Including the outermost extensions, one gets 1.77 10^{-10} erg cm^{-2} s^{-1}. The important thing to emphasize is that our images are absolutely calibrated, so that every pixel provides an absolute flux value for various interference filters in use. It is always possible to use isophotal contours to obtain the total flux values.

For the "same" bright area $F(\mathrm{H}\beta) = 2.07\ 10^{-11}$ erg cm^{-2} s^{-1}, leading to a Balmer decrement of 8.21, so that we derive $E(B-V) = 1.05$ (in the case B assumption). This result is not so discrepant with above radio determination. For the same region, $F([\mathrm{NII}]) = 4.53$ (4.64 including the outermost extensions) 10^{-10} erg cm^{-2} s^{-1}, leading to the following intensity ratios: $F([\mathrm{NII}])/F(\mathrm{H}\beta) \sim 22$, instead of 17.58 (Acker93, but this "discrepancy is not significant due to the irregular shape of the planetary nebula); $F([\mathrm{NII}])/F(\mathrm{H}\alpha) = 2.65$ instead of 2.5 (Acker93). $F([\mathrm{OIII}]) = 3.86$ (3.93 with extensions) 10^{-10} erg cm^{-2} s^{-1} leading to $F([\mathrm{OIII}])/F(\mathrm{H}\beta) = 18.7$ (13.5 Acker93) and $F([\mathrm{OIII}])/F(\mathrm{H}\alpha) = 2.26$ (1.92 Acker93). $F([\mathrm{SII}]6717) = 3.66$ (3.93) 10^{-12} erg cm^{-2} s^{-1}; $F([\mathrm{SII}]6731) = 3.85$ (3.97) 10^{-12} erg cm^{-2} s^{-1}, so that the average intensity ratio equals 0.95.

3.20. NGC 6853 – PNG 060.8 – 03.6

The Dumbbell nebula has been extensively investigated by several teams during the last two decades (Hua & Louise 1970, 1981; Moreno-Corral et al. 1992). However, one may ask a question as to whether this planetary nebula has so far revealed all its overall structure.

New monochromatic images (Figs. 20) were taken in Hα, Hβ, [NII] and [OIII] emission lines. The overall dimensions are much larger than the 12′ field of view offered by the 120-cm telescope (f/6). NGC 6853 probably should have the same intrinsic morphology as Sh 1-89 (Hua 1997) but seen pole-on, the outer emission corresponding to an equatorial confinement (gravitational breaking) due to a massive central star. Our monochromatic pictures suggest shock mechanism, along with the ISM influence. An extended halo was detected around the "dumbbell" centre, with this particularity that this halo is not the same in Hα, [NII] or in [OIII]. Radial structures show up with "cometary dust" features outwards. A prominent dusty patch crosses the [OIII] image, which has not the same morphology as in the two other lines. Even S^{++} ion is seen outwards, of course quite much fainter. Due to the non-photometric conditions during the absolute

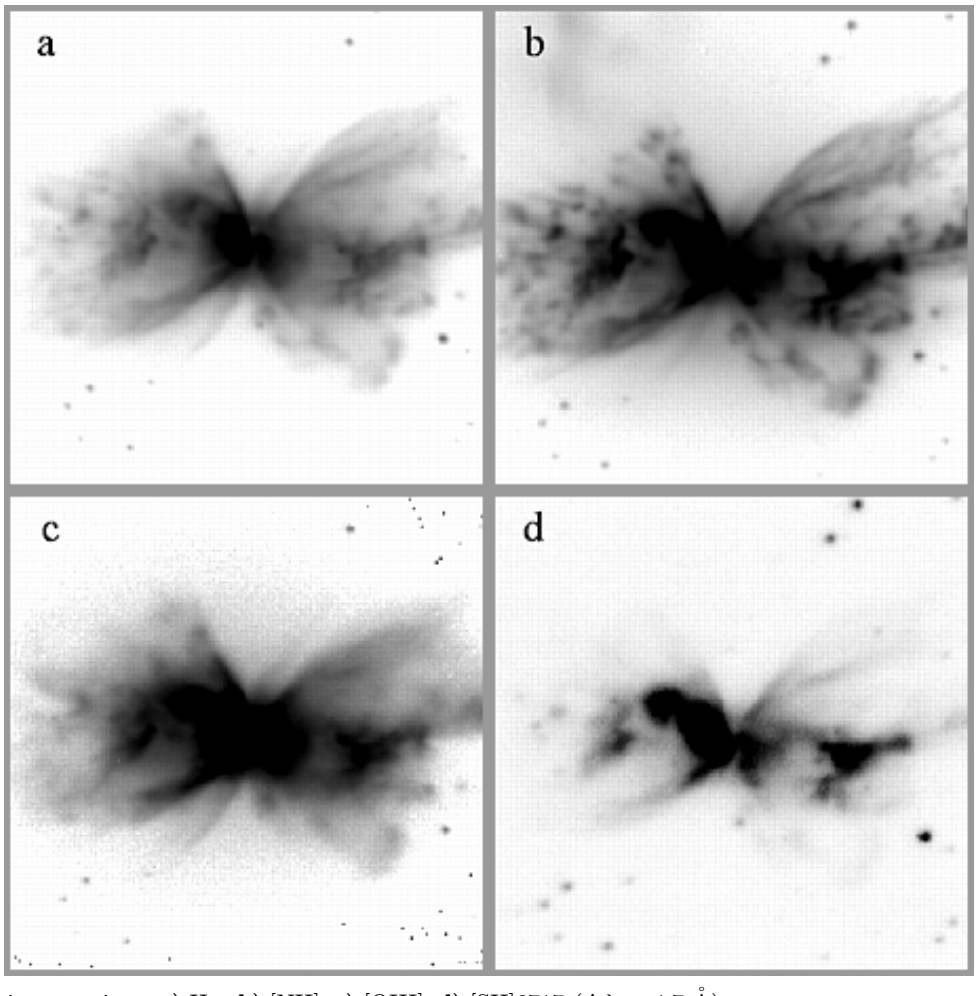

Fig. 19. NGC 6302 inner regions. **a)** Hα. **b)** [NII]. **c)** [OIII]. **d)** [SII]6717 ($\Delta\lambda = 4.7$ Å)

calibration, we prefer not to provide uncertain flux values, and do hope to be able to do such calibration shortly in better conditions. Nonetheless, attempts to estimate ionized mass were done using the measured Hα dimensions. The major axis of the bright main nebula (470″) would infer $M_{\rm i} = 3.89\ 10^{-3}\ \epsilon\ N_{\rm e}$, at the distance of 262 pc. Assuming $\epsilon \times N_{\rm e} = 0.3 \times 1000$, one gets 1.16 $M_{\odot}$. The overall diameter is much larger (720″), leading to $M_{\rm i} = 0.11\ \epsilon \times N_{\rm e}$, so that the total ionized mass would be 3.3 $M_{\odot}$ if $\epsilon \times N_{\rm e} = 0.3 \times 100$.

3.21. SaWe 3 − PNG 013.8 − 02.8

This outstanding planetary nebula displays a bipolar shape in Hα, and [NII] (Figs. 21) more obviously than in [OIII]. In absence of some useful parameters (distance, radio flux, etc.) we could only provide the absolute fluxes (Table 3). The Hα/[NII] intensity ratio slightly differs with spectroscopic data (see Table 2); as a matter of fact, after superimposing the [NII] and Hα images, we measured this ratio varying from 0.7 (outermost area) to 3.6 (in the central bright filament).

3.22. SaWe 4 − PNG 014.7 − 11.8

The Hα image (Fig. 13b) shows two small condensations over a roundish (40″ diameter) and diffuse nebula emitting a flux $F(\mathrm{H}\alpha) = 4.44\ 10^{-13}$ erg cm^{-2} s^{-1}. Without knowledge of its distance, we cannot derive the corresponding ionized mass.

4. Summary

We have reported the first detection of secondary structures (faint halo, outermost emissions) around some galactic planetary nebulae using narrow bandpass interference filters centred at Hα, [NII]6583 and [OIII]5007 Å. Alike NGC 6720 (Ring Nebula), such outer structures, which give the PNe a mulptiple-shell morphology (Chu et al. 1987), could be understood as relics of primary ejections when the PN progenitors experience the AGB-phase. Alternatively, these newly detected emissions could result from the projection of the loop/bubble structures situated in each side of the nebula "waist" (which generally appear as elliptical/rectangular bright cores, e.g. Sh 1-89 in Hua

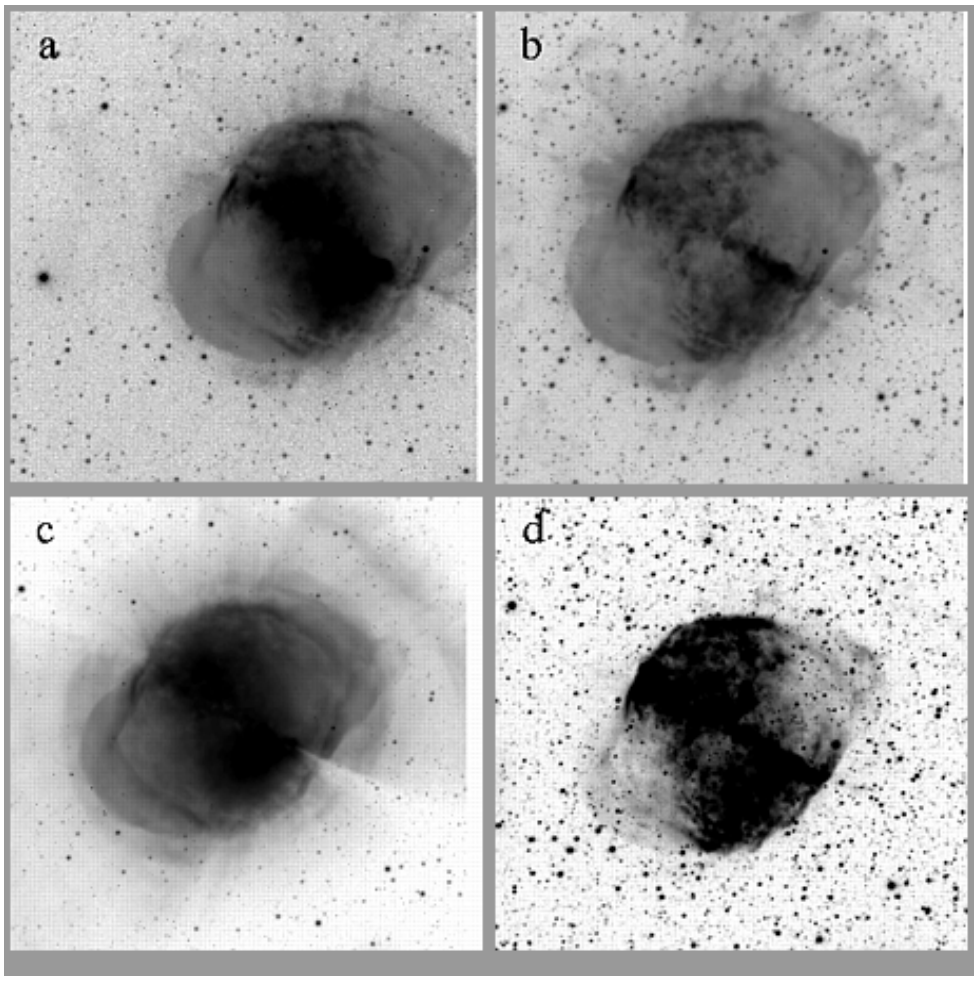

Fig. 20. NGC 6853. **a)** Hα. **b)** [NII]. **c)** [OIII]. The well-known "dumbbell" shape of the central area is not reproduced here. The emission structures of the outer halo detected in these images do not have the same origin. The dusty patch is well outlined in [OIII]. The overall dimensions should be larger than our present field of view (12′)

1997). This interpretation is supported by the ellipsoidal shell models proposed by Zhang & Kwok (1998) taking into account the pole-to-equator density gradient. Viewed along its major axis, Sh 1-89 would display a multiple-shell structure, of which the Ring nebula (NGC 6720) is a good representative. The slight asymmetrical shape (interpreted as due to the influence of the interstellar medium, Soker 1997) would result from the angle between line-of-sight and the PN major axis. Seen edge-on, NGC 6720 would display bipolarity with a dumbbell-shape, alike Sh 1-89 (Hua 1997), or a double-cone-shape, alike SaWe 3 in the present study. Meanwhile, such outer emissions raise the problem of overall ionized mass for planetary nebulae which depends upon several parameters so far not well known. In the majority of cases, $N_{\rm e}$ is not measured, and the distance is very poorly determined. Moreover, most of the PNe are far from homogeneous. For this reason, we have provided ionized masses in terms of $\alpha \times \epsilon\ N_{\rm e}$, α being a numerical factor which mainly depends upon the PN distance, and Hα radius (numerical values in Table 2, Col. 11). Absolute calibrations are available for the PNe reported in the present study in FITS files for further investigations. In addition, a new emission nebula was detected in the field of NGC 3699, which presumably emits stronger in [NII] and [OIII] than in Hα.

Acknowledgements. CTH would like to express his thanks to Drs. J.B. Hearnshaw, W. Tobin (University of Canterbury, Christchurch) and M. Clark (Lake Tekapo Superintendant) for their kind hospitality during several observing runs at MJUO, and INSU-CNRS for travel grants. We are indebted to the MSSO Program Committee for allocation of the ATT 2.3 metre telescope at Siding Spring Observatory. We thank Prof. S. Kwok of the University of Calgary for his pertinent comments on using the radio data to compare with the optical measurements. We thanks Prof. J. Lequeux for his advices to improve the manuscript.

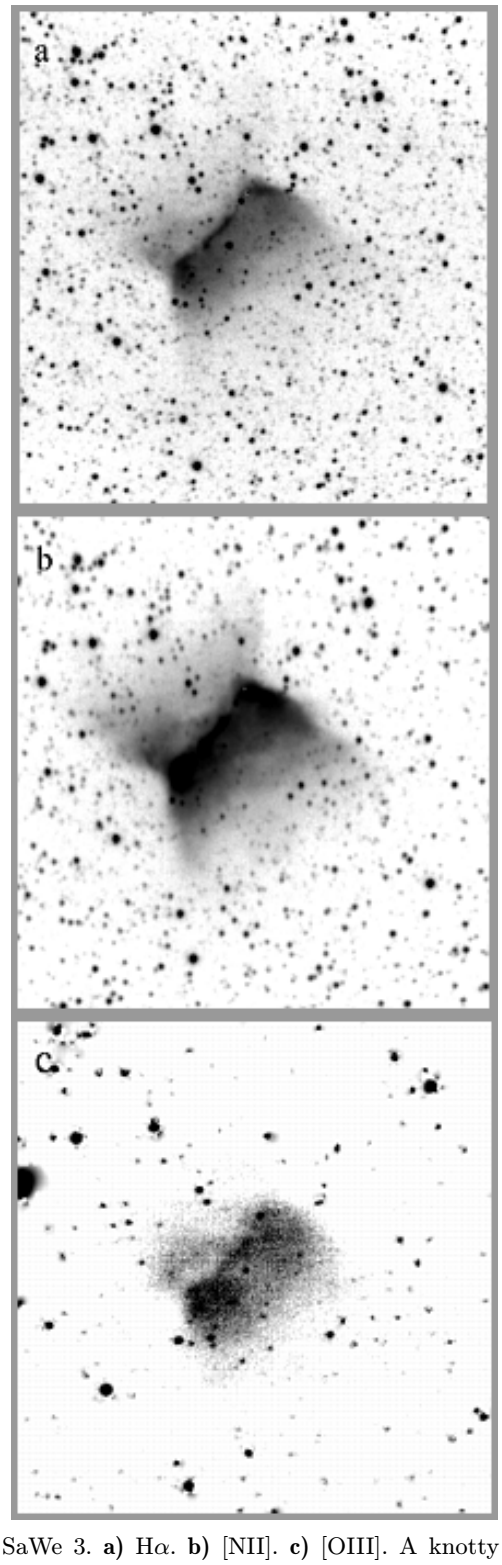

Fig. 21. SaWe 3. **a)** Hα. **b)** [NII]. **c)** [OIII]. A knotty core is surrounded with extended EW diffuse emissions. Probably seen edge-on, SaWe 3's intrinsic structure should resemble Sh 1-89

References

Acker, Ochsenbein F., Stenholm B., Tylenda R., Marcout J., Schon C., 1993, The Strasbourg-ESO Catalogue of Galactic Planetary Nebulae. ESO Publishing (Acker93)

Balick B., 1987, AJ 94, 671

Bond H.E., Livio M., 1990, ApJ 355, 568

Cahn J.H., Kaler J.B., 1971, ApJSS 22, 319 (CaKa71)

Cahn J.H., Kaler J.B., Stanghellini L., 1992, A&AS 94, 399 (CKS92)

Chevalier R.A., 1994, in Asymmetrical Planetary Nebulae, Oranim - University of Haifa, Israël, Harpaz & Soker (eds.), p. 240

Chu Y.-H., Jacoby G.H., Arendt R., 1987, ApJS 64, 529

Dgani R., Soker N., 1997 (preprint)

Dopita M.A., et al., 1997, ApJ 474, 188

Dopita M.A., Hua C.T., 1997, ApJS 108, 515

Drilling, 1983, ApJ 270, L13-15

Duncan J.D., 1937, ApJ 86, 496

Dwarkadas, Balick, 1998 (preprint)

Hua C.T., 1997, A&AS 125, 355

Hua C.T., Nguyên-Trong T., 1983, A&A 117, 272

Hua C.T., Grundseth B., Maucherat A.J., 1993, A&AS 101, 541

Jewitt D.C., Danielson B.E., Kupferman P.N., 1986, ApJ 302, 727

Kaler J.B., 1974, AJ 79, 594

Kupferman P.N., 1983, ApJ 266, 689

Kwok S., Purton C.R., FitzGerald M.P., 1978, ApJ 219, L125

Kwok S., 1982, ApJ 258, 280

Kwok S., 1994, PASP 106, 344

Livio M., 1982

Maciel W.J., 1984, A&AS 55, 253

Meatheringham S.J., Dopita M.A., Morgan D.H., 1988, ApJ 329, 166

Millikan A.G., 1974, AJ 79, 1259

Moreno-Corral M.A., López-Molina M.G., Vásquez-R G.A., 1992, Rev. Mexicana Astron. Astrof. 24, 151

Pascoli G., 1992, PASP 104, 350

Peimbert M., 1981, in Physical Processes in Red Giants? Reidel Publ., Iben Jr. & Renzini (eds.), p. 409

Peimbert M., Torres-Peimbert S., 1983, IAU Symposium 103. London, Reidel, Dordrecht

Pottasch S.R., 1984, Planetary Nebulae. Reidel, Dordrecht

Pottasch S.R., 1989, A&A 205, 248

Renzini, 1981, Physical Processes in Red Giants. D. Reidel Publ.

Schwarz H., Corradi R., Melnick J., 1992, A&AS 96, 23

Shklowskii I.S., 1956, Astron. Zh. 33, 315

Stewart, 1898, Harvard Annals 60, 163

Tüg H., 1975, AAS 39, 67

Vassiliadis E., Wood P.R., 1994, ApJSS 92, 125

Warner J.W., 1974, PASP 86, 885

Zhang C.Y., 1988, Ph.D. Thesis

Zhang C.Y., Kwok S., 1998, ApJS (in press)